

Politecnico di Torino

Department of Environment, Land and Infrastructure Engineering

Master of Science of Georesources and Geoenergy Engineering

A.y. 2024/2025

Optimization of Carbon Dioxide storage in a Depleted hydrocarbon Reservoir

Supervisor:

Candidate:

Prof. Vera Rocca

Milton Carlos Boane

Table of Contents

| 1. | Introducti | on | 3 |
|----|------------|---|----|
| 2. | Theoretica | al background of CO2 storage | 5 |
| | 2.1 Ove | erview of CO2 storage worldwide | 5 |
| | 2.2 Sto | rage typologies and storage mechanisms | 8 |
| | a) | Storage capacity | 9 |
| | b) | Injectivity | 12 |
| | c) | Integrity | 13 |
| | 2.2.1 | Trapping mechanisms | 13 |
| | a) | Structural and Stratigraphic Trapping (Physical Trapping) | 14 |
| | b) | Residual Trapping | 15 |
| | c) | Solubility Trapping | 16 |
| | d) | Mineral Trapping | 16 |
| | 2.3 D | Definition of CO ₂ properties | 17 |
| | a) | Density behavior | 18 |
| | b) | Viscosity behavior | 19 |
| | c) | Compressibility factor, z at different temperature | 20 |
| | d) | Formation volume factor, Bg behavior | 21 |
| | 2.4 C | CO ₂ Storage strategies | 22 |
| | 2.5 N | Jumerical simulation of CO ₂ storage | 24 |
| 3. | Case Stud | у | 26 |
| | 3.1 Mo | del description | 27 |
| | 3.1.1 | Fluid System and Phase Behavior Modeling | 29 |
| | 3.1.2 | Relative permeability functions | 31 |

| | 3.1.3 D | ynamic Model Implementation and Scenarios Design33 |
|----|-----------------|---|
| | 3.1.4 Si | mulated scenarios |
| | a) | Base Case (No Aquifer)35 |
| | b) | Weak aquifer + injector in gas zone case |
| | c) | Strong aquifer + injectors in gas zone |
| | d) | Base case + injection in water zone (No aquifer)38 |
| | e) | Weak aquifer + injector in water zone case |
| | f) | Strong aquifer + injectors in water zone |
| | 3.2 Resi | ults discussion40 |
| | a) | Depletion phase |
| | b) | Pressure profile in different phases of simulation42 |
| | c) timesteps | Saturation distribution in different scenarios at different simulation 43 |
| | d) | CO2 component dissolved in brine |
| 4. | Conclusion | n51 |
| 5 | References | 53 |

List of Figures

| Figure 1: Operational and planned capture capacity. Source |
|--|
| https://www.iea.org/data-and-statistics/data-tools/ccus-projects-explorer |
| Figure 2: Operational and planned capture capacity distribution. Source: https://www.iea.org/data-and-statistics/data-tools/ccus-projects-explorer |
| Figure 3: Operational and planned projects type capacity. Source https://www.iea.org/data-and-statistics/data-tools/ccus-projects-explorer |
| Figure 4: Example of unconfined aquifer used for CO2 storage. A case of Utsira formation in North Sea. Source: IPCC, 2005 (p.202) |
| Figure 5: Trapping mechanisms evolution on the time (IPCC, 2005)14 |
| Figure 6: Phase diagram for CO2. Copyright © 1999 ChemicaLogic Corporation, 99 South Bedford Street, Suite 207, Burlington, MA 01803 |
| Figure 7: CO2 density behaviour varying pressure and temperature19 |
| Figure 8: CO2 viscosity behaviour varying pressure and temperature20 |
| Figure 9: CO2 compressibility factor, varying pressure and temperature21 |
| Figure 10: CO2 formation volume factor, varying pressure and temperature 22 |
| Figure 11: Illustration of CCS. Source: Gassnova, n.d |
| Figure 12: Simulation grid block. Fluids saturation |
| Figure 13: Stratigraphic heterogeneity. Different stacking layers representing fluid regions |
| Figure 14: Relative permeability curves for CH4-Brine32 |
| Figure 15: Relative permeability curves for CO2-Brine |
| Figure 16: Wells placement in base case scenario: injectors in gas zone36 |
| Figure 17: Injection wells not flooded by encroached water after depletion36 |
| Figure 18: Injection wells not flooded by encroached water after depletion in presence of a weak bottom aquifer |
| Figure 19: Injection wells not flooded by encroached water after depletion in presence of a strong bottom aquifer |
| Figure 20: Wells placement in base case scenario: injectors in water zone39 |
| 21: Field gas production and CO2 injection profiles40 |

| Figure 22 Field gas production and CO2 injection profiles with correspondent cumulative water production |
|---|
| Figure 23: Pressure profile at field scale |
| Figure 24: Saturation distribution on scenarios with CO ₂ injection in gas zone |
| Figure 25: Saturation distribution on scenarios with CO ₂ injection in gas zone, one representative cross-section selected |
| Figure 26: Saturation distribution on scenarios with CO2 injection in water zone |
| Figure 27: Saturation distribution on scenarios with CO2 injection in water zone, one representative cross-section selected |
| Figure 28: CO2 dissolved in brine. The cases in which the injectors are in gas zone |
| Figure 29: CO ₂ dissolved in brine. The cases in which the injectors are in water |
| zone48 |
| List of Tables |
| |
| List of Tables |
| List of Tables Table 1: Main active commercial CCS projects |
| List of Tables Table 1: Main active commercial CCS projects |
| List of Tables Table 1: Main active commercial CCS projects |
| List of Tables Table 1: Main active commercial CCS projects |
| List of Tables Table 1: Main active commercial CCS projects |

Abstract

The rising on carbon dioxide concentration into the atmosphere brings a need to a large-scale deployment of mitigation technological measures. CO₂ geological storage in Depleted Gas Reservoirs is a secure strategy for long-term CO₂ sequestration. This thesis focuses on the optimization of CO₂ storage performance in a depleted gas reservoir, focusing into maximizing the amount of CO₂ dissolved in formation brine. The analysis is done assuming that during simulation period, the main trapping mechanisms operating are structural and solubility trapping, hence, the impact of the other trapping mechanisms that may be acting, is assumed negligible.

Compositional Eclipse-300 was used to build a reservoir simulation model, to be able to handle the multi-phase flow and fluid composition change behavior during injection. The study investigated the impact of different injection strategies: injecting into residual gas zone of a depleted reservoir and injecting into the water zone. Additionally, the geological setup was changed by adding an active analytical bottom aquifer with different strengths to assess its influence on CO₂ dissolution.

A 10-year injection period was followed by an approximately 100-year simulation run to analyze long term dissolution. The main finding was that injection well placement is a major factor affecting the amount of CO₂ dissolved in brine. Injecting directly into the water zone benefits dissolution. On the other hand, the presence of the aquifer negatively impacts the results when injecting into the gas zone, while having a negligible impact when injecting into the water zone.

In the best-case scenarios studied, approximately 11% of the total injected CO₂ was dissolved in the brine after nearly 100 years post-injection (i.e., after stopping injection).

As a way forward for this work, a further investigation can be proposed to quantify the amount of CO2 that was trapped due to residual and mineral trapping mechanisms during the analyzed timeframe.

I sincerely thank the **ERB-ENI Management** for providing me opportunity to conclude a master's degree.

My deepest appreciation goes to my supervisor, **Prof. Vera Rocca**, for her **patience and guidance**.

Finally, thank you to my family for their support, especially my mother, Violeta Mudumane (posthumously), for instilling in me a strong belief in education.

Chapter 1

Introduction

The urgency for effective measures to address the global climate change challenges has driven Carbon Capture and Storage (CCS) into a position of critical importance. The continuous rise in atmospheric carbon dioxide (CO₂) concentrations, which is observed its steep rise since around the 1970's and primarily derived from anthropogenic industrial activities and fossil fuel combustion, presents a significant risk to global climate stability (Benson & Cole, 2008). CO₂ injection for geological storage has evolved as important solution for long-term mitigation of emissions by sequestrating large volumes of captured CO₂ into stable subsurface formations (Gassnova, n.d.). A massive deployment of this technology will positively impact on meeting international decarbonization targets while ensuring a sustainable energy future supply, particularly in regions where industrial emissions remain high.

The fundamental scopes of CO₂ geological storage are to ensure the permanent containment of the injected CO₂ in identified and characterized geological structure with enough capacity to hold gigatonnes of CO₂, and with optimized injection rates to maximize the use of the reservoir volume while maintaining safe operating pressures. Among many options of geological formation typologies for CO₂ storage, depleted hydrocarbon reservoirs offer the advantage of pre-existing historical data that ensures the existence of caprock integrity and enough volume capacity, making them preferred choice for accelerated and economical deployment (Gozalpour, 2005).

CO₂ storage projects feasibilities are studied by means of numerical simulation using available modelling tools such as Eclipse[®] simulation software, a Schlumberger product. The approach involves building a robust 3D static model that represents the main geological features of the site and, a dynamic reservoir model that can reproduce the complex, multi-phase fluids flow processes occurring over time of production and/or injection. The CO₂-hydrocarbon-water phase behaviour, relative permeability changes, pressure evolution, and the specific trapping mechanisms, are specially modelled using compositional reservoir simulators packages (Peter et al., 2022). These models allow to test different development strategies (well configurations, operational constraints) to ensure maximum storage efficiency.

This thesis focuses on the optimization of CO₂ storage in a synthetic gas reservoir, utilizing a reservoir simulation, the compositional Eclipse-300. The work aims to investigate the performance of injected CO₂ dissolution in formation brine under different injection strategies. This include evaluating the impact of CO₂ dissolution when injected on residual gas zone after a gas reservoir is depleted, or directly in water zone below the gas-water-contact (GWC), considering varying the model's geological setup by incorporating an active analytical bottom aquifer with different strengths and then identifying the optimal injection plan that maximizes the amount of CO₂ dissolved in brine after a fixed amount of CO₂ was injected for a period of 10 years, and its dissolution is analysed for approximately 100 years after injection ceases.

With the findings of this work, is expected to provide valuable insights for maximizing the benefit of solubility trapping mechanisms by applying adequate injection strategy in a depleted gas reservoir and ultimately contribute with knowledge to global decarbonization challenge.

Chapter 2

Theoretical background of CO₂ storage

2.1 Overview of CO₂ storage worldwide

The CO₂ injection is reported to have been active in North Americas since the 1970s, when it began to be used for Enhanced Oil Recovery (EOR) operations (IEA, 2024). Transitioning from EOR to a large-scale commercial CCS was made in the middle of 1990s, with the launch of the Sleipner project in Norway in 1996, that was dedicated in injecting CO₂ in geological formation with the main objective of storage (IEA, 2024). The Sleipner project is designed to inject around 1 million tons per annum (Mtpa) of CO₂ separated from natural gas (IEA, 2024).

Currently there is a strong growth in CCS projects catalyzed by the urgent need to address the climate change and the global commitment to meet the net-zero emission by mead 21st century. The table 1 below shows the main commercial CCS projects active, their location and design capacity.

| CCS Project | Country | Capacity (Mtpa) | Note |
|--------------------|-----------|----------------------------|---------|
| Century Plant | USA | 5.0 - 8.4 | EOR |
| Shute Creek | USA | ~7.0 | EOR |
| Gorgon | Australia | ~4.0 (Design) | Storage |
| Quest | Canada | ~1.0 | Storage |
| Sleipner | Norway | ~1.0 | Storage |
| Snøhvit | Norway | ~0.7 | Storage |
| Northern Lights | Norway | 1.5 (Phase 1) | Storage |
| Bozhong 26-6 | China | (1.5 Mt total lifetime) | EOR |

Table 1: Main active commercial CCS projects

In the figure 1 are synthetized the operational and planned CO₂ capture capacity worldwide. There are considered all operational, under construction and planned CO₂ capture facilities with an announced capacity of more than 10⁵ tones/year and an announced timeline. The data is obtained by summing the estimated capacity of capture, full chain and CCS projects in the IEA CCUS Projects Database. The 2025e includes announced capacity which could come online by the end of 2025 according to IEA CCUS Projects Database (last updated 30th April 2025).

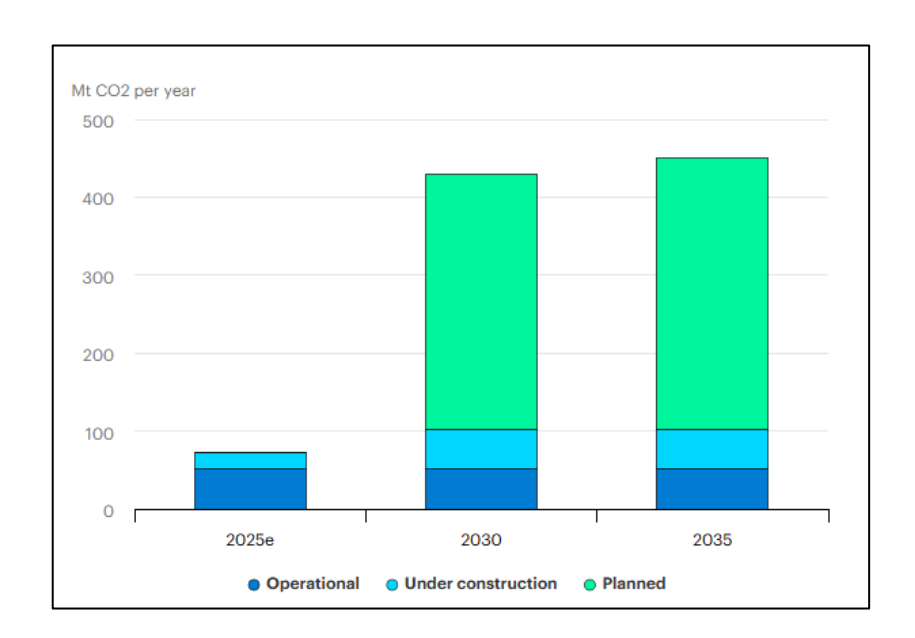


Figure 1: Operational and planned capture capacity. Source: https://www.iea.org/data-and-statistics/data-tools/ccus-projects-explorer

According to IEA CCUS Projects Database, in terms of planed capacity up to 2030, it is expected to have significant growth in European countries, moving from the 5.6% global contribution in 2025, to 30.9% by 2030. The figure 2 below shows how CCS project capacity is distributed worldwide and what is expected near future trend according to plane, based on reported in IEA CCUS Projects Database.

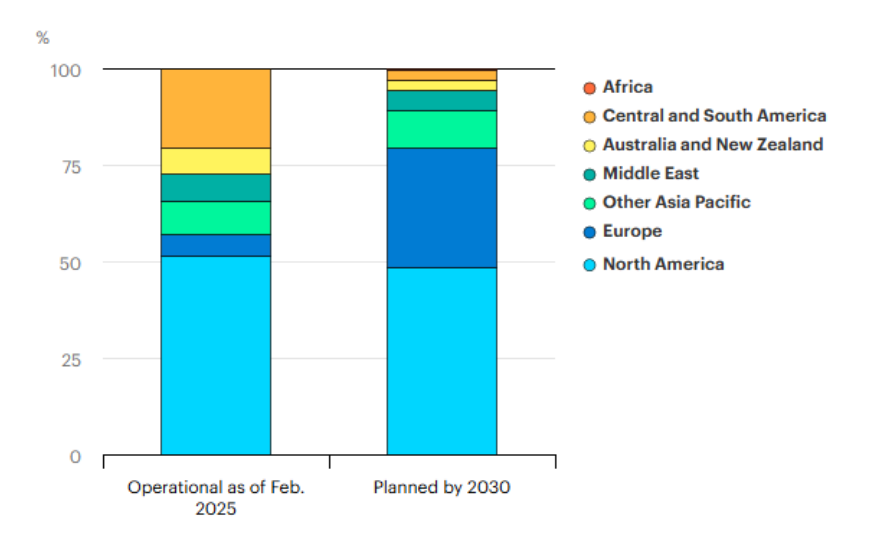


Figure 2: Operational and planned capture capacity distribution. Source: https://www.iea.org/data-and-statistics/data-tools/ccus-projects-explorer

The figure 3 is showing that in future, major growth will be dedicated to CCS projects for CO₂ capture, and for CO₂ storage, with higher focus into CO₂ storage projects, that is planned to move from the 15 Mtpa in 2025, to 537.2 Mtpa in 230, and even higher by 2035, reaching 634.9 Mtpa of CO₂ injected in storage projects.

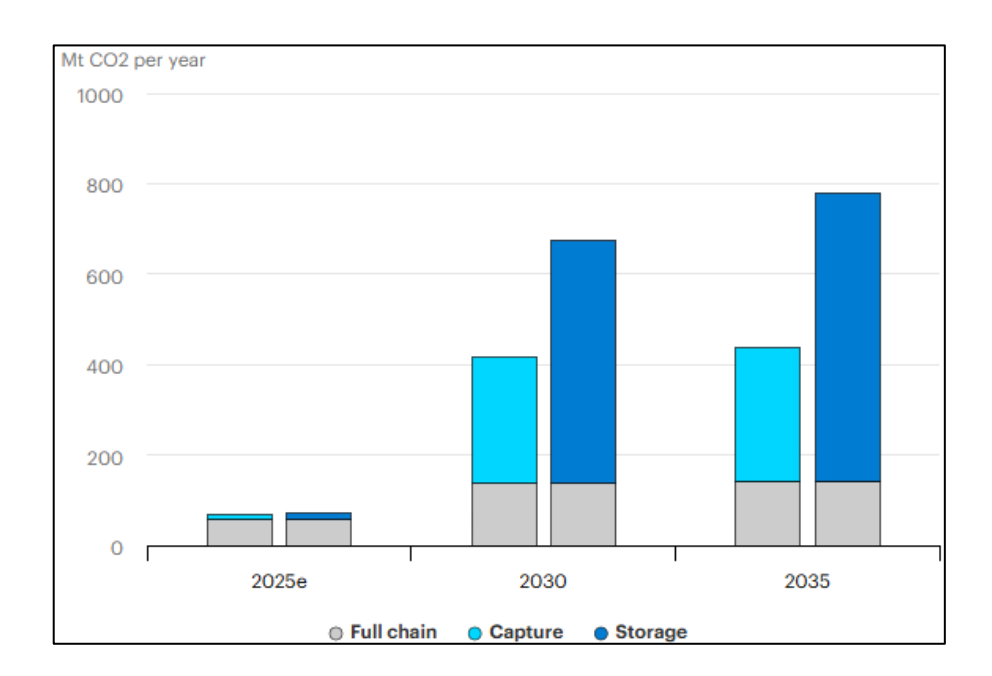


Figure 3: Operational and planned projects type capacity. Source: https://www.iea.org/data-and-statistics/data-tools/ccus-projects-explorer

2.2 Storage typologies and storage mechanisms

Several types of geological formations are suitable for storage, even if each have different characteristics, advantages and drawbacks (IPCC, 2005; Bachu, 2008). Depleted oil and gas reservoirs are well studied geological formations and suitable typology for CO₂ storage. Their history of containing hydrocarbons, which proves the existence of caprock integrity, and the potential to reuse existing operational infrastructure, makes them advantageous option (Bachu, 2008). Deep saline aquifers are another considered as good geological formation for storing CO₂, with the advantage of offering a widespread availability and vast storage potential capacity (Benson & Cole, 2008). Another advantage for using these formations is the non-conflicting with human needs, as the brine contained in it, is unsuitable for

human or agricultural use (Michael et al., 2010). Unmineable coal seams are also considered as an option, as CO₂ adsorbs onto the coal matrix, often displacing methane. Their normally low permeability can present significant operational challenges by limiting injectivity (IPCC, 2005). Other options under investigation may emerge once technical and economic barriers will be overtaken. One example are the basaltic formations which show potential for rapid CO₂ mineralization, but they're not yet considered as viable (IPCC, 2005).

A geological formation to be selected for CO₂ storage, must fulfil several geological and technical requirements. It must have enough capacity to hold the desired amount of CO₂ to be injected, a sealing low permeable layer (caprock) that prevents injected CO₂ from migrating away from storage formation, and a good permeability to ensure injectivity.

a) Storage capacity

This refers to the total volume of pore space within the rock formation that is available to contain the injected CO₂. It is a measure of how much CO₂ can be stored, making it an important factor in determining the viability of a project. The capacity of a formation is highly related to the gross volume, net to gross and porosity of formation (Ahmed, 2006). Highly porous rocks like sandstone and carbonate rocks are ideal for storage because they can contain a significant volume of fluid due to the high available pore volume. The depth of the reservoir is also essential for ensuring a large storage capacity, as deeper the reservoir, the higher the pressure, which allows CO₂ to exist in a supercritical phase maximizing in this state, the amount (mass) of CO₂ that can be stored in a volume of pore space, as supercritical, denser CO₂ occupies a much smaller volume than gaseous CO₂ (IPCC, 2005). 800 m are considered the ideal minimum depth of a formation for storage.

Assessment procedures to determine capacity depend on the geological medium in which is being evaluated (depleted hydrocarbon reservoir, confined or unconfined aquifer). The storage capacity of a depleted reservoir is assumed to be the same as the Initial Hydrocarbon in Place (IPCC, 2005), however if we consider not all reservoir gas or oil is produced, and, that part of the porous space that was previously occupied by gas or oil, during production is filled by water that is not entirely replaced by the injected CO₂ (Gozalpour et al., 2005), we can easily predict slightly lower volume available for storage compared to the original hydrocarbon in place.

Storage capacity in a depleted reservoir and confined aquifer is calculated by the equation 1 adapted from petroleum engineering (Bachu, 2008).

$$CO_{2}Vomule_{at\ SC} = \frac{GBV \times NTG \times \emptyset \times (1 - S_{w,r})}{FVF}$$
(1)

$$NTG = \frac{\sum_{i=1}^{n} h_i}{H} = \frac{Net \ reservoir}{Gross \ reservoir}$$
 (2)

Where:

GBV - gross bulk volume of the formation, the total volume of the storage rock.

NTG – net to gross ratio, percentage of the rock favorable for storage.

Ø - effective porosity, a fractional volume of the interconnected pores.

 $S_{w,r}$ – residual water saturation, accounting for the immobile water in the pores.

FVF - formation volume factor, to convert reservoir volume to surface conditions.

In unconfined aquifer storage formation, the calculation of storage capacity does not consider the entire volume of the formation (Bachu, 2008). Unconfined aquifers are vast underground formations not delineated by specific geometry, laterally unconfined, and these layers are filled by brine (Benson & Cole, 2008; Michael et al., 2010). The injected CO₂ rises due to density gradient with the brine, until it is trapped by the caprock (IPCC, 2005). Once the plume reaches the impermeable caprock, it stars a lateral movement following the less resistant pathway, the larger interconnected pores (Benson & Cole, 2008). This movement will not be uniform, and the plume will only occupy a small part of the entire formation. From this, it becomes clear that interpreting the storage capacity of unconfined aquifer as the total volumetric capacity of the formation, may lead to a big overestimation (Bachu, 2008). As solution, an efficiency factor is applied to the calculation. This efficiency factor represents the fraction of the total formation pore volume that will be occupied by the injected CO₂ (IPCC, 2005). This factor is normally as low as values between 0.1 to 0.4 (IEAGHG, 2018).

$$M_{CO_2} = A \times h \times NTG \times \emptyset \times \rho_{CO_2} \times \Delta P \times (\beta_r + \beta_f)$$
 (3)

Where:

 M_{CO_2} - is the regional aquifer storage capacity

A – is the area of aquifer

h - is average thickness of aquifer

 ho_{CO_2} - is CO_2 density at reservoir condition

 ΔP – is the pressure variation due to injection

 β_r and β_f – are rock and fluid compressibility respectively

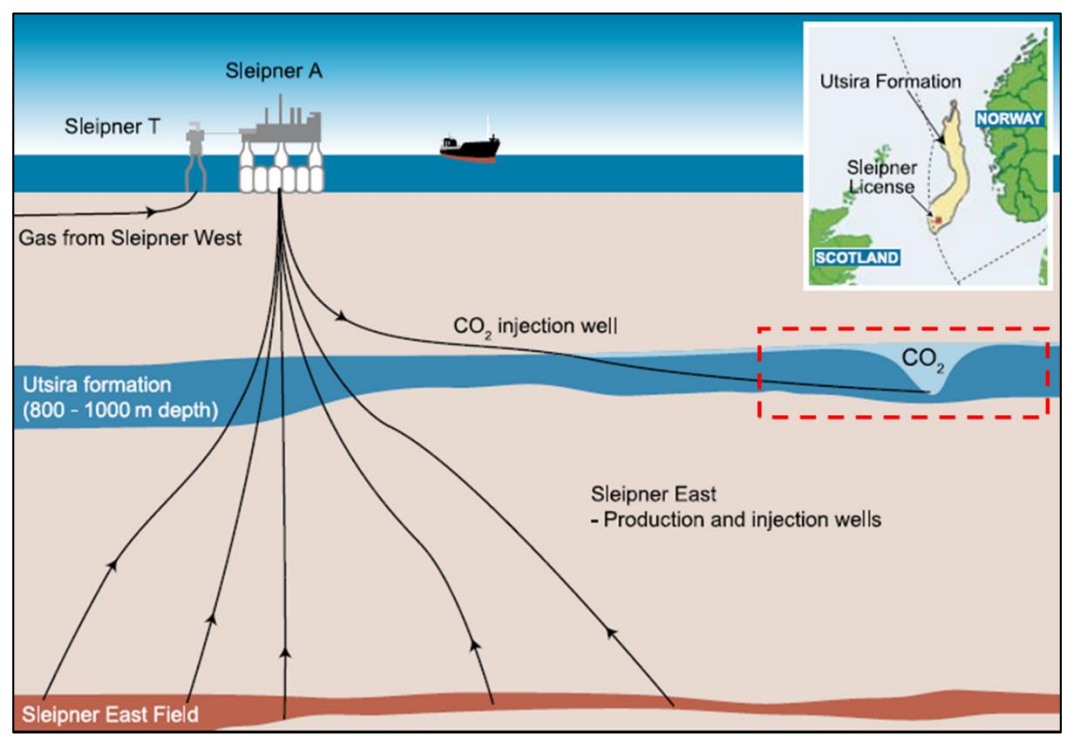


Figure 4: Example of unconfined aquifer used for CO2 storage. A case of Utsira formation in North Sea. Source: IPCC, 2005 (p.202).

b) Injectivity

It is the ability of formation reservoir to receive the injected rate of CO₂. A site with high injectivity allows for a smooth, continuous injection process without requiring excessive pressure, reducing in this was the operational costs, and managing the risk of wellbore failure or induced seismicity (Ahmed, 2006). Injectivity is directly related to the rock formation permeability, being the permeable rocks, the ones allowing the injected CO₂ to spread out and be distributed efficiently within the formation due to the well-connected pore spaces (Ahmed, 2006). A high-permeability formation is necessary to achieve the high injection rates required for large-scale industrial projects. A low permeable and low injectivity formation, would require a higher number of injecting wells, consequently impacting on the project's complexity and cost (IPCC, 2005).

c) Integrity

Site integrity is related to the presence of a sealing caprock, with the capacity to geologically secure a long-term trapping of injected CO₂ (IPCC, 2005). A caprock is a low-permeability rock layer that acts as a physical barrier that prevents the buoyant CO₂ from migrating upward toward the surface (Benson & Cole, 2008). Rocks like shale or dense evaporites (e.g., salt) make excellent caprocks due to their very low permeability and non-connected pores (IPCC, 2005). The integrity of this caprock is very important, and it must not have major faults or fractures that could act as a pathway for CO₂ to leak (Bachu, 2008). Furthermore, the overall geological setting must be stable and secure, with a history of long-term containment of fluids, as evidenced by natural gas or oil reservoirs that have held hydrocarbons for millions of years (IPCC, 2005; Bachu, 2008).

2.2.1 Trapping mechanisms

Containment of injected CO₂ into a geological formation relies in series of progressive in time, and permanent trapping mechanisms. These mechanisms are essential for preventing the gas from migrating back to the surface. The very primary containment is achieved through physical means, called structural and stratigraphical trapping mechanism, followed by processes that immobilize the CO₂ through geochemical reactions, which are, residual gas trapping, solubility trapping and mineral trapping (IPCC, 2005).

Figure 5 shows how different trapping mechanisms operates in time.

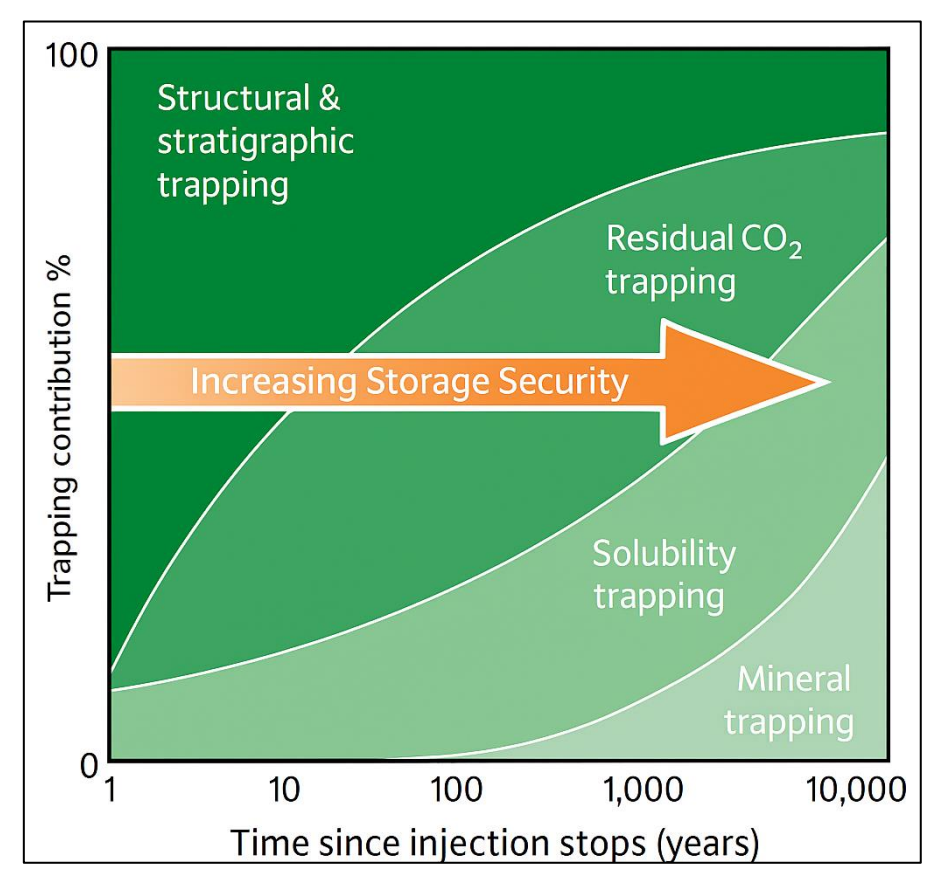


Figure 5: Trapping mechanisms evolution on the time (IPCC, 2005).

a) Structural and Stratigraphic Trapping (Physical Trapping)

This is the primary trapping mechanism that is observed immediately after CO₂ is injected. After is injected, the buoyant CO₂ migrates upwards until it is physically blocked by an impermeable or very low-permeability layer known, as previously mentioned, as "caprock". The CO₂ then spreads laterally beneath this sealing rock, becoming trapped in structural highs or domes in the reservoir rock. Natural accumulations of CO₂ found worldwide, which have been trapped for millions of years, provide evidence of the long-term effectiveness of this mechanism.

The caprock's sealing capacity is a capillary phenomenon where the high capillary pressure within the rock's very small, interconnected pore throats resists the entry of the non-wetting fluid (IPCC, 2005). The seal will fail, and leakage will occur, only if the buoyant force of the non-wetting fluid exceeds a critical pressure

value, called threshold displacement pressure or breakthrough pressure. Breakthrough pressure is the minimum pressure required to force the non-wetting fluid to form a continuous, connected phase flowing through the largest interconnected pore throats (Smith, 1966). This is distinct from the capillary entry pressure, which is a lower pressure that allows the non-wetting fluid to enter the largest, but not necessarily interconnected, pores (Hildenbrand et al., 2002). Therefore, the sealing efficiency of a caprock is quantified by the maximum vertical column height (h) of gas it can safely store before the buoyant pressure at the reservoir caprock interface becomes equal to the breakthrough pressure. This value can be measured directly in a lab using a "step-by-step" test (Purcell, 1949).

b) Residual Trapping

As the CO₂ plume migrates through the porous rock, some of it is immobilized in the pore spaces by capillary forces and interfacial tension effects, leaving behind disconnected and not movable "bubbles" of CO₂ trapped in the wetting phase fluid (brine) (IPCC, 2005; Benson & Cole, 2008). This mechanism can immobilize a significant amount of CO₂ (Michael et al., 2010). Formations with high permeability heterogeneity are more prone to residual trapping effectiveness, as this prevents the CO₂ from forming into a single, mobile phase. This trapping mechanism turns the CO₂ into an immobile state, further reducing the risk of upward migration (Bachu, 2008).

The effectiveness of the capillary trapping mechanism is mainly supported by hysteresis. In the context of CCS, hysteresis is referred to as the dependence of relative permeability and capillary pressure on the saturation history of the fluids (non-wetting, CO₂ and wetting, brine) (Benson & Cole, 2008). During the injection phase drainage occurs, where CO₂ displaces brine, and as the plume migrates, water flows back into the pore spaces that were previously occupied by CO₂, in a process called imbibition (Michael et al., 2010). This imbibition process causes the

disconnection of the CO₂, creating the immobile residual gas (bubbles) saturation (IPCC, 2005; Bachu, 2008).

c) Solubility Trapping

After time CO₂ is injected, it will start dissolving into formation water (brine). This process prevents the CO₂ to exist in the reservoir as a separate phase and becoming no longer buoyantly movable. This process can take decades or thousands of years. The dissolution of CO₂ into water forms carbonic acid (H₂CO₃), which dissociates into bicarbonate (HCO₃⁻) and carbonate (CO₃²⁻) ions making the CO₂ gas to become aqueous phase, eliminating its possibility of migrating as free phase. Dissolution of CO₂ in brine is dependent in pressure, temperature, and salinity: high pressure favors dissolution, high temperature and high-water salinity is unfavorable to dissolution (IPCC, 2005).

After brine becomes more and more saturated by CO₂ it rises slightly its density to approximately 1% higher than the original unsaturated brine (IPCC, 2005). The density difference between saturated and original brine creates an instability, and the denser brine starts a downwards movement, while less dense and unsaturated brine rises to replace it, in a natural circulation called free convection. This process plays an important role in the long-term storage of CO₂ in saline aquifers and enhances long-term storage security (IPCC, 2005).

d) Mineral Trapping

As described in dissolution trapping, the dissolved CO₂ will make brine denser, and it will move down in a convective movement. Part of it will form ionic species as the rock dissolves, and some part may be transformed in stable carbonates minerals in a process called mineral trapping mechanism.

This trapping mechanism is relatively much slower if compared to the others, taking even thousands to millions of years to occur. It involves certain chemical

reaction between dissolved CO₂ and minerals in the rock formation resulting in stable solid carbonate minerals, effectively converting CO₂ into a rock-like form that is permanently isolated from the atmosphere (IPCC, 2005). This is the most secure form of keeping CO₂ trapped into a geological formation (Gunter et al., 1993; IPCC, 2005).

2.3 Definition of CO₂ properties

Carbon dioxide is a chemical element made up of molecules that each have one carbon atom double linked covalently to two oxygen atoms. It is a tiny percentage of the atmosphere (around 370 parts per million) and is very important for Earth's biochemical cycles since plants take it in during photosynthesis, and it released when the animals breathe, when fossil fuels burns, or during fermentation (Schlesinger & Bernhardt, 2013). At standard temperature and pressure (STP), CO₂ is a gas that is colorless, non-flammable, and has a smell that is slightly unpleasant. It is heavier than air and can be dangerous to human health at high levels, even though it is naturally present in modest amounts (OSHA, 2020).

The physical state of CO₂ is determined by temperature and pressure. The phase diagram of CO₂ in figure 6, illustrates the pressure and temperatures at which transition between solid, liquid, gas and supercritical phases, occur. Triple point of CO₂, where solid, liquid, and gas phases simultaneously exist in equilibrium, occurs at -56.56°C and 5.18 bar. Below triple point pressure, solid CO₂ transits directly into gas (sublimation). At the temperature of 31.0°C and pressure of 73.8 bar (critical point), liquid and gas phases cannot be distinguished. At temperatures and pressures higher than critical point, CO₂ transits to a supercritical state where it shows coexistence of both liquid and gas properties, with a gas like viscosity and liquid-like density. The high density and low viscosity of CO₂ at supercritical state allows for efficient storing process in geological formations.

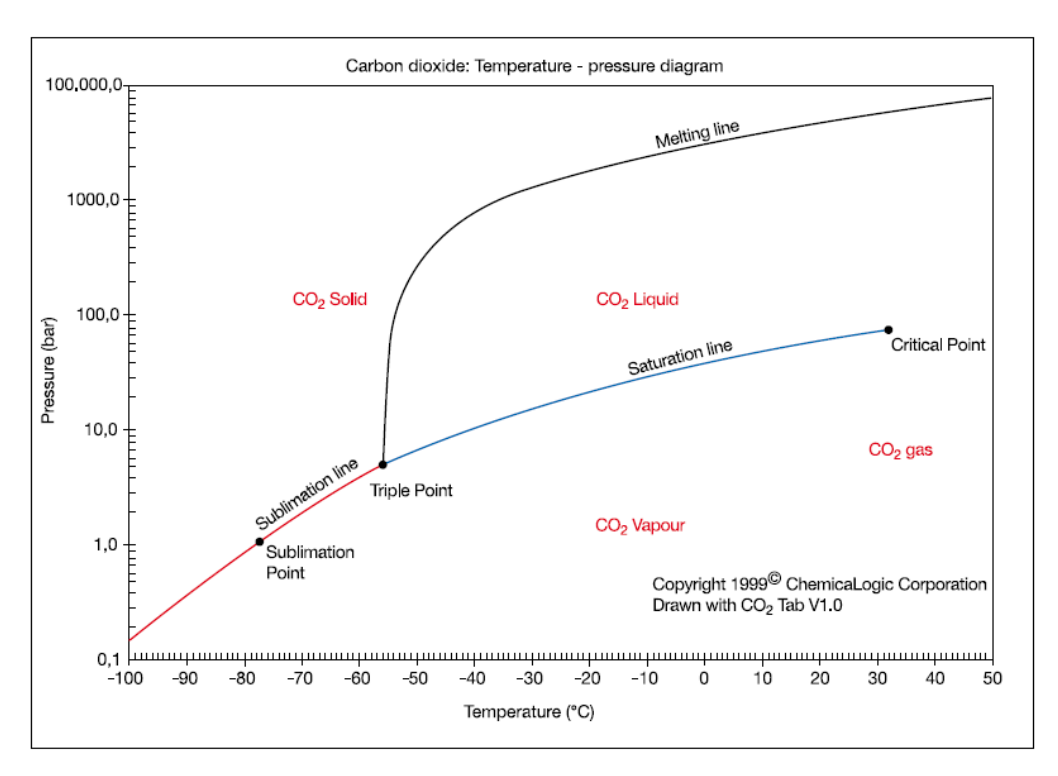


Figure 6: Phase diagram for CO2. Copyright © 1999 ChemicaLogic Corporation, 99 South Bedford Street, Suite 207, Burlington, MA 01803

The thermodynamic properties of CO₂ (viscosity, density, compressibility factor and formation volume factor) changes significantly with a slight change in pressure and temperature near the critical point.

a) Density behavior

The curves of CO₂ density versus pressure, at temperatures below the critical temperature (T< 31.1 °C) shows sharp increase when pressure values are between 50 – 75 bar. It indicates a transition from gas to liquid like behavior; high compressibility at gas-like density and nearly incompressible at liquid-like density. Close to critical temperature, the curve (curve in gray color) shows more visible inflection indicating behavior of critical fluid at the pressure values close to the CO₂ critical pressure.

Curves at temperatures above 31.1 °C, shows more smooth increase of density with pressure. See figure 7 below.

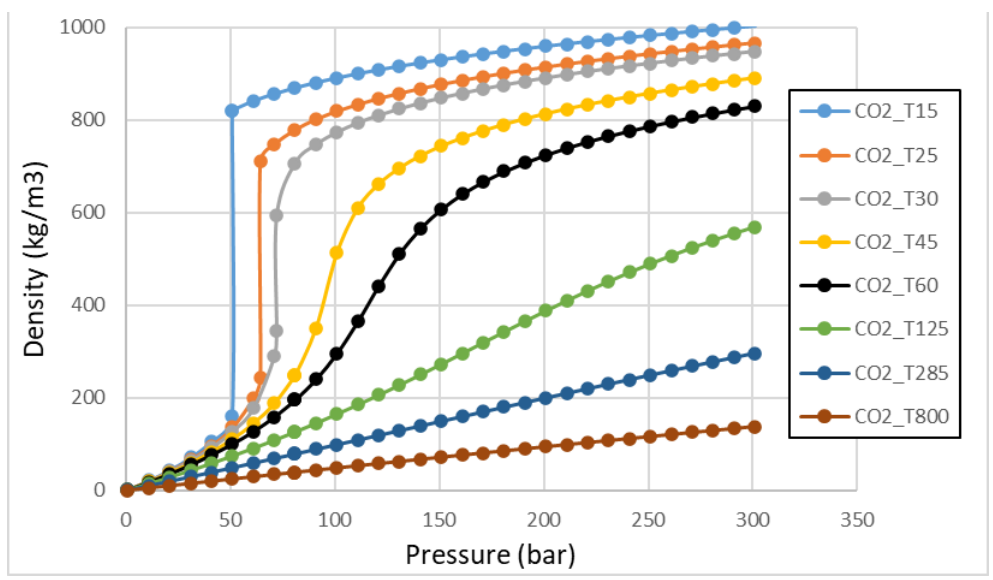


Figure 7: CO2 density behaviour varying pressure and temperature

b) Viscosity behavior

The viscosity of CO₂ rises with increasing pressure (at constant temperature), exhibiting especially sharp changes near the critical point. In the immediate vicinity of the critical conditions, particularly at temperatures around 31.1 °C, the fluid's resistance to flow rises steeply. Once CO₂ enters the supercritical state, its viscosity levels off and shows much less dependence on temperature. These trends illustrate the dramatic shift in CO₂'s transport properties as it moves from gas-like behavior into the supercritical fluid state. See figure 8.

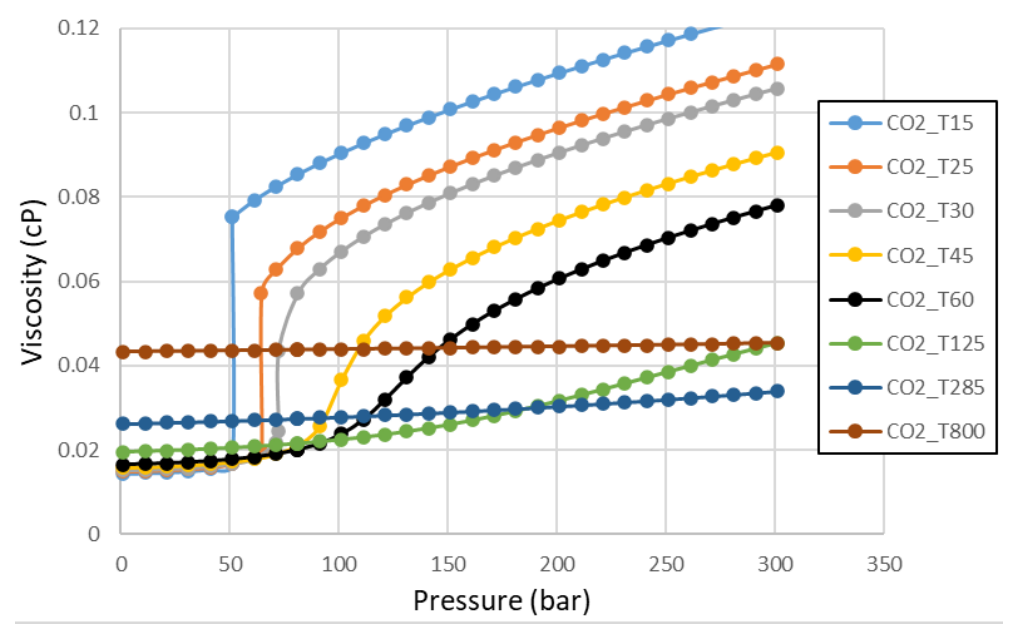


Figure 8: CO2 viscosity behaviour varying pressure and temperature

c) Compressibility factor, z at different temperature

Below and close 31.1°C, Z-factor decreases sharply while pressure increases from 0 to ~70 bar, showing high deviation from ideal gas compressibility behavior. The minimum Z-factor value for each temperature is increasing as the temperature increases. For the higher temperature cases, Z-factor is nearly 1, indicating that gas compressibility is nearly ideal gas behavior even at higher pressure. See the plots in figure 9.

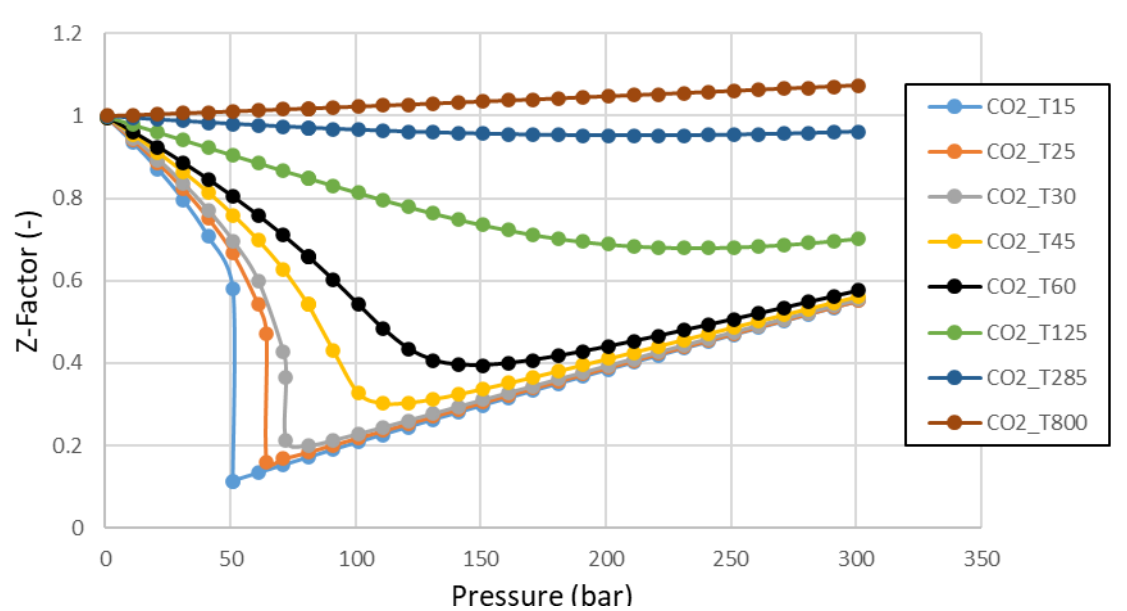


Figure 9: CO2 compressibility factor, varying pressure and temperature

d) Formation volume factor, Bg behavior

Bg decreases with increasing pressure. At pressure values below critical, the rate of decrease is much rapid. After critical pressure, all curves continue to decrease, but in more linear behavior as pressure continues to increase. At higher temperatures (T285 and T800), Bg values are at its highest, indicating that at high temperatures, CO₂ is more gas-like and less dense. See the plots illustrated in figure 10.

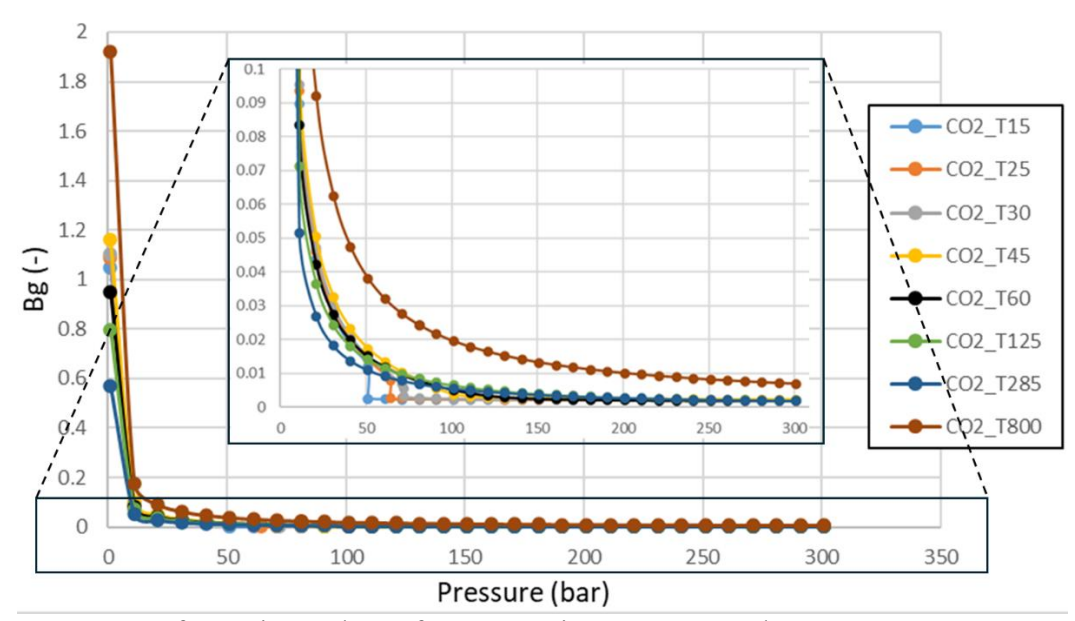


Figure 10: CO2 formation volume factor, varying pressure and temperature

2.4 CO₂ Storage strategies

CO₂ storage process starts at the point of emission like large fossil fuel power plants, cement factories, or natural gas processing structures. At these facilities, CO₂ is captured from other gases by using chemical, physical, or membrane-based capture technologies. According to the IEA Greenhouse Gas R&D Programme (2007), it is attractive to capturing CO₂ from large point sources because of the large achievable economies of scale. After CO₂ is separated, it is compressed and transported to a designated geological injection site (IPCC, 2005).

Three main methods for transporting CO₂ from a collection site to injection site are commonly considered (pipelines, ships, and trucks/rail). Pipelines are normally considered as cost-effective method for transporting big volumes of CO₂ for long distances (Metz et al., 2005). CO₂ is compressed to a supercritical or liquid state to reduce its volume and allow for efficient transport through the pipeline. Figure 11 illustrates the main chain composing a CCS project.

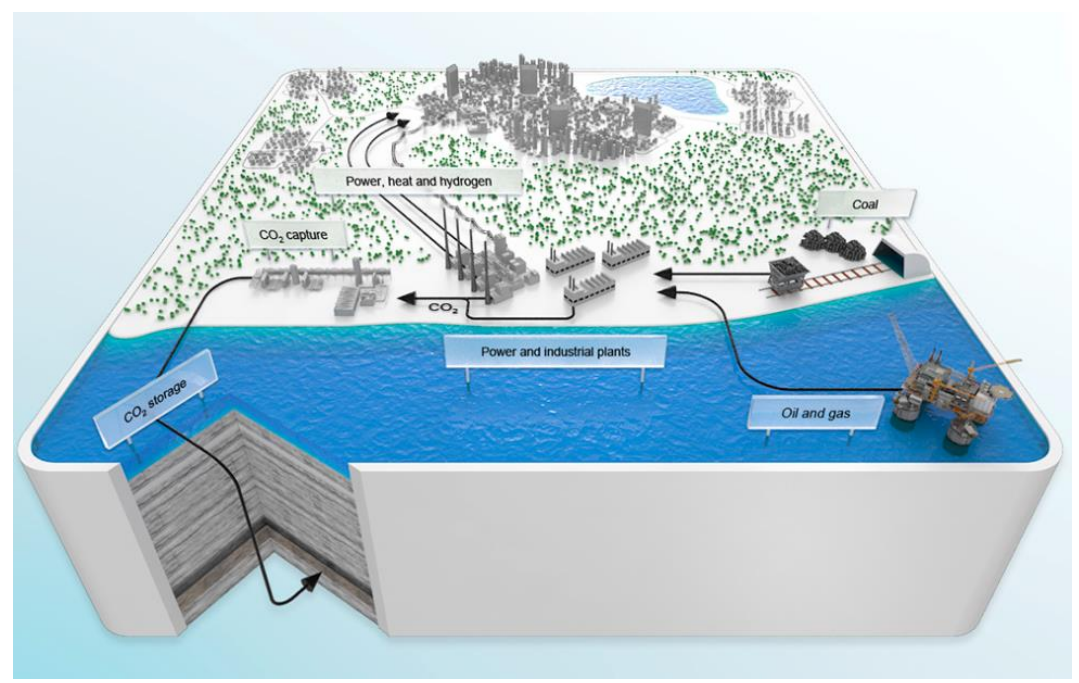


Figure 11: Illustration of CCS. Source: Gassnova, n.d.

Ideally, CO₂ is injected at minimum depth of 800 meters, as pressure and temperature are usually above critical conditions so, the fluid is at supercritical state (IPCC, 2005). Once injected, CO₂ becomes buoyant due to density gradient with formation brine and capillary forces until it is trapped by the series of trapping mechanisms, where structural trapping is the primary one operate.

The safety and effectiveness of underground storage projects need to be assessed. Monitoring technologies like seismic surveys and pressure monitoring are used to, respectively, keep track of migration of injected CO₂ plumes in the subsurface and detect potential risks of overpressure and caprock failure. Advanced technological tools like InSAR (Interferometric Synthetic Aperture Radar) are available to monitor ground deformation to denunciate subsurface changes related to injection activities. CO₂ storage monitoring helps to builds public acceptance to CCS technology also is a compliance measure within the regulatory standards.

Nevertheless, underground CO₂ storage is subject to risks such as leakage, induced seismicity and chemical interactions between CO₂-saturated brine and

reservoir rocks. Existence of these risks are to be minimized, by means of modeling techniques that can allow early detection and mitigation.

2.5 Numerical simulation of CO₂ storage

Numerical modeling of CO₂ injection is the primary method used to predict the behavior, migration, and long-term fate of the injected plume, forming the basis for site validation, injection monitoring and risk assessment (IPCC, 2005). This process, known as reservoir simulation, relies on creating a discretized 3D geological model that is representing the storage formation and its overlying caprock. Static petrophysical properties, such as porosity, permeability, and capillary entry pressure, are populated spatially in the 3D geological model (static). These data are derived from geological and geophysical interpretations and measurements (Bachu, 2008). The simulation then models the dynamics of CO₂ injection, that typically is a buoyant, low-viscosity supercritical fluid, which displaces the native brine, creating a complex, multiphase flow problem (Benson & Cole, 2008).

Fluid flow behavior in the porous medium follows a set of coupled, non-linear partial differential equations that accounts for the conservation of mass principle (IPCC, 2005). Darcy's Law is the fundamental equation describing the relationship between fluid velocity, pressure gradients, and rock permeability.

$$v_i = -\frac{k_{ri} * k}{\mu_i} * (\nabla p_i - g\rho_i)$$
(4)

Where:

v – fluid *velocity*

k – absolute permeability

k_r – relative *permeability*

μ - viscosity

 ∇p - pressure gradient

g - gravitational constant

 ρ - density

i - phase

This is extended to a multiphase system by introducing relative permeability and capillary pressure functions (Benson & Cole, 2008). These functions are critical as they govern the complex interactions between the immiscible fluids (non-wetting CO₂ and wetting brine) and describe how they flow competing for pore space, which in turn controls plume migration and the effectiveness of key trapping mechanisms like residual (capillary) trapping (Michael et al., 2010).

Due to the geological heterogeneity and the non-linearity of the governing equations, these models cannot be solved analytically. Instead, they are "handled" numerically using simulators that employ spatial discretization techniques, such as the Finite Difference or Finite Volume methods (Michael et al., 2010). These methods transform the continuous partial differential equations into a large system of algebraic equations, which are then solved iteratively for each grid cell at discrete time steps. This numerical approach allows for the simulation of complex processes including advection, viscous fingering, dissolution, and pressure buildup, providing quantitative estimates of storage capacity, security, and the long-term maturation of storage resources (IPCC, 2005; Ringrose & Meckel, 2019)

Chapter 3

Case Study

This chapter presents a detailed case study utilizing a synthetic, "Eclipse-300" compositional reservoir simulation (the Schlumberger E300 software) model to investigate the dynamics of CO₂ injection for the primary purpose of optimizing injection strategy to enhance CO₂ dissolution in native brine. While the model is synthetic, its geological architecture and petrophysical properties are inspired by the Gullfaks Field, with significant simplification for academic investigation purpose. The simulation model was previously adapted for being used in Eclipse simulation lessons, on its E100 version, reason why there was a need for converting into E300 conserving its initial volumes. The reservoir was considered a gas reservoir made of Mateine (CH₄).

The study aims to analyze and compare different injection strategies with the objective to identify the best scenario to optimize a long-term storage security by dissolution trapping mechanism. Focus will be on quantifying the dissolution of injected CO₂ into the formation brine during and after injection. As already described in sections above, this mechanism is important as it significantly increases storage security by ensuring the CO₂ remains non-buoyant and immobilized over geological timescales.

For such investigation, is used the compositional simulator E300 as it employs an equation of state to explicitly model the inter-component mass transfer and phase behavior of CO₂ dissolving into the aqueous phase, a process the black-oil model E100 cannot accurately represent. As first step, a base case scenario will be set up involving two simulation phases: depletion phase at first stage to produce the in-

situ gas, then injection phase to inject the CO₂ into the depleted reservoir. Then different other scenarios (changing the geological setup and injection location points) will be considered, and the results will be analyzed and compared.

3.1 Model description

The structural configuration of the synthetic model is a simple, inclined stratigraphic unit with consistent dip, and without complex faulting. This simplified structure was chosen intentionally to isolate the effects of stratigraphic heterogeneity on CO₂ plume migration, removing the complicating influence of fault related flow barriers. The primary trapping mechanism is structural, provided by the up-dip closure of the formation, which would be sealed by an overlying, impermeable caprock (not explicitly modeled but assumed to be present). The reservoir properties are summarized in table 2 below.

| Parameter | Value | |
|-------------------|------------------|--|
| Grid size | 14 x 36 x 14 | |
| Cell height range | 3.25 – 29.06 m | |
| Porosity | 0.01 – 0.15 p.u. | |
| Permeability | 10 – 250 mD | |
| NTG | 0.04 - 0.65 | |
| Pressure at Datum | 200 bars | |
| Res. Temperature | 75 °C | |
| GWC | 2030 m | |

Table 2: Reservoir properties

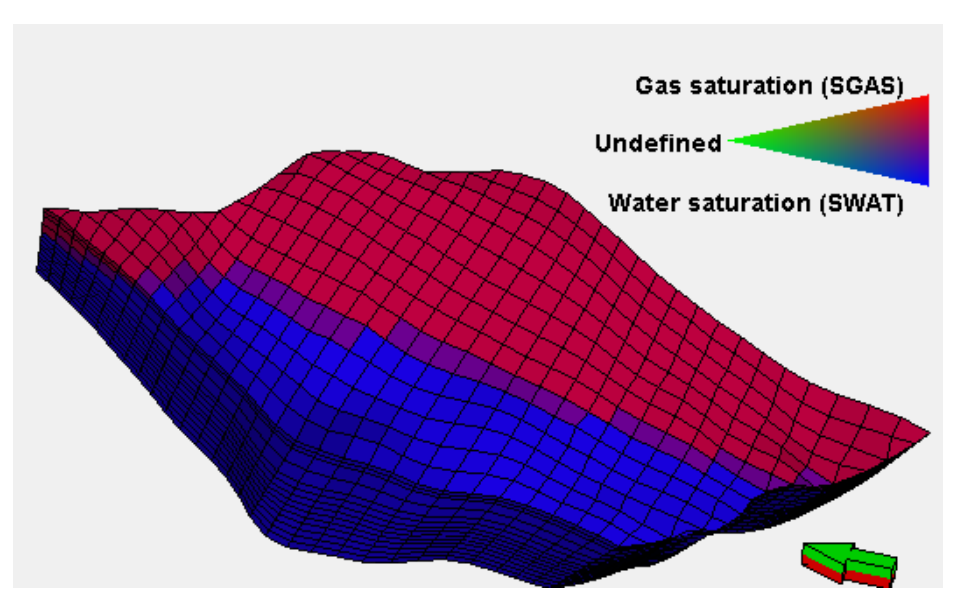


Figure 12: Simulation grid block. Fluids saturation

The reservoir is stratified and divided into five distinct geological layers, or petrophysical regions, stacked vertically, representing a depositional sequence with significant heterogeneity among the regions, with properties ranging from high-quality reservoir rock to very low-quality rock, however, no inside region heterogeneities are considered, meaning, single petrophysical values are distributed in each region. figure 13 shows the 5 regions contained in the synthetic model.

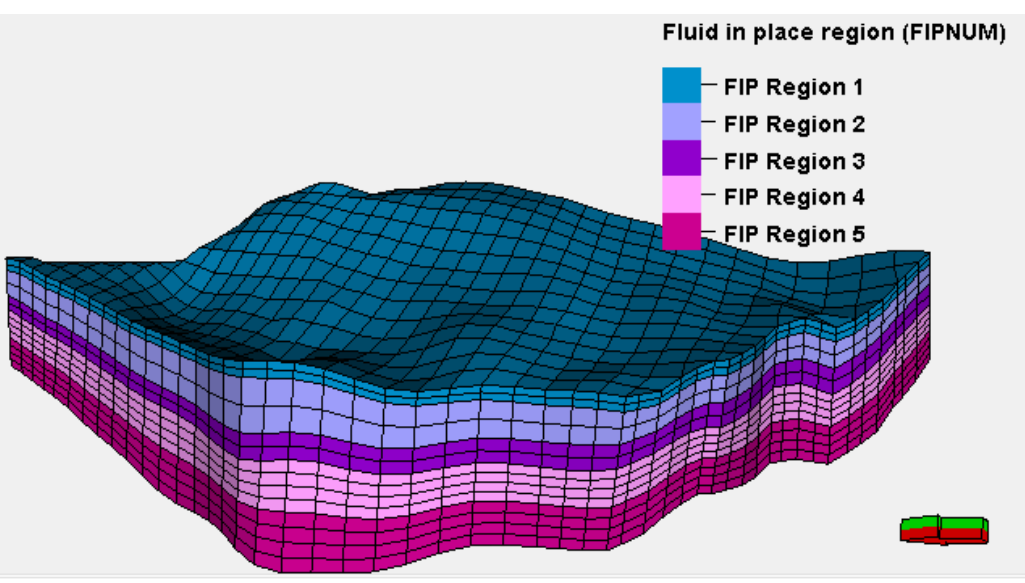


Figure 13: Stratigraphic heterogeneity. Different stacking layers representing fluid regions

Porosity ranges from a low of 1% in the low permeable layers to a high of 15% in the primary storage zone. In the same manner, permeability varies from 10 mD to 250 mD. This permeability contrast, of a little over one order of magnitude between the best and worst layers is the most dominant factor controlling fluid flow. Nevertheless, this layered heterogeneity is not expected to lead to poor vertical sweep during injection.

| Region ID (FIPNUM) | Porosity (\phi) | Net-to-Gross (NTG) | Permeability (kx, mD) |
|-----------------------|-----------------|-----------------------|-----------------------|
| Region 1 | 0.15 | 0.65 | 250 |
| Region 2 | 0.07 | 0.39 | 100 |
| Region 3 | 0.01 | 0.04 | 10 |
| Region 4 | 0.10 | 0.54 | 100 |
| Region 5 | 0.01 | 0.04 | 10 |

Table 3: Petrophysical distribution per layer

3.1.1 Fluid System and Phase Behavior Modeling

The synthetic model is initialized with conditions representing a gas reservoir with high Matein content in its composition (98% Matain and 2% water). The phase behavior of the fluid is modeled using the Peng-Robinson EOS, a robust model for calculating phase equilibrium for multi-component mixtures at high pressures and temperatures (Span & Wagner, 1996). The fluid model includes components for CH₄, CO₂ and H₂O, and EOS parameters (critical pressure, critical temperature, and acentric factor), are defined for each component. The water salinity is accounted via PVTW and SALINITY Eclipse keywords. The option for CO₂ solubility in water is enabled by the Eclipse 300 keyword "CO2SOL". The simulator then,

calculates the fluid properties like density and viscosity within the range of conditions expected during injection (Linstrom & Mallard, 2023).

$$P = \frac{RT}{v - b} - \frac{a * \alpha}{v(v + b) + b(v - b)}$$
 (5)

The parameters a (molecular volume), b (attraction forces), and α (correction factor) are calculated using the critical properties of the fluid.

$$a = 0.45724 \frac{R^2 T_c^2}{P_c} \tag{6}$$

$$b = 0.0778 \frac{RT_c}{P_c} \tag{7}$$

Where:

P - is the pressure.

R - is the universal gas constant.

T - is the absolute temperature.

v - is the molar volume of the fluid.

a - is a parameter associated with the attractive forces between molecules

b - is a parameter associated with the repulsive forces between molecules

 α (or α (T)) is a temperature-dependent parameter

 T_r – is reduced temperature

k − is a constant dependent of acentric factor

| E o C Down motor | E | oS Parameter valu | es |
|----------------------|-----------------|-------------------|--------|
| EoS Parameter | CH ₄ | CO ₂ | H_2O |
| T. Critical (°K) | 190.56 | 304.2 | 647.3 |
| P. Critical (Bar) | 45.99 | 73.8 | 220.55 |
| M. Weight (kg/kmol) | 16.04 | 44.01 | 18.02 |
| Acentric Factor | 0.0142 | 0.225 | 0.344 |

Table 4: EoS parameters used in simulation. Source: NIST Chemistry WebBook (Linstrom & Mallard, n.d.). https://webbook.nist.gov

3.1.2 Relative permeability functions

While the EOS governs fluids phase behavior, relative permeability functions describe how multiple fluid phases flow simultaneously are related among them within the porous rock. The model defines a set of two-phase relative permeability curves for the gas-water system employing the keywords SWFN (water saturation vs. relative permeability to water) and SGFN (gas saturation vs. relative permeability to gas) tables, which together specify the two-phase relative permeability curves.

Two saturation function tables are used: CH₄ – Brine relative permeability table is used during depletion phase and CO₂ – Brine relative permeability table is used during injection phase. The CO₂ -Brine relative permeability curve was retrieved from a technical paper published by Jeong et al. (2021), with tittle "Effect of the Flow Rate on the Relative Permeability Curve in the CO₂ and Brine System for CO₂ Sequestration".

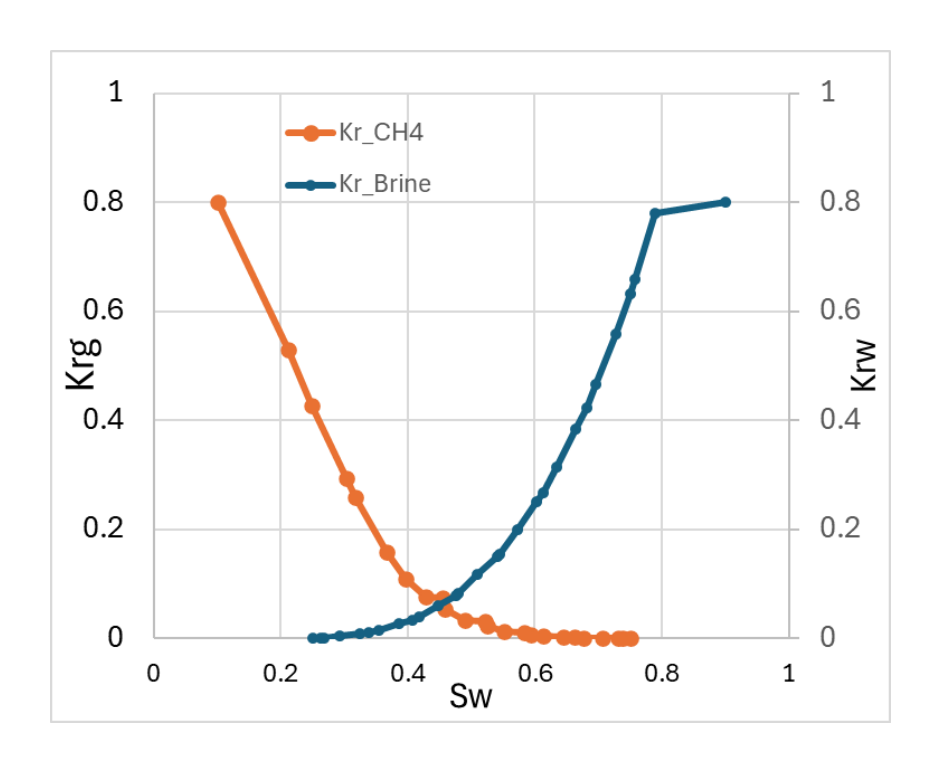


Figure 14: Relative permeability curves for CH4-Brine

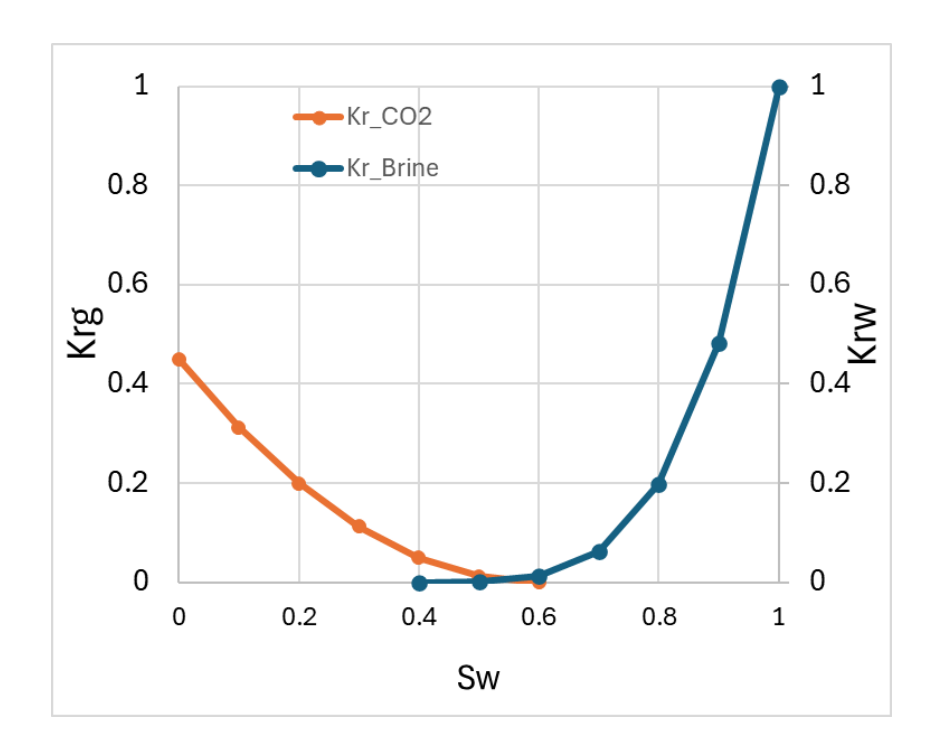


Figure 15: Relative permeability curves for CO2-Brine

The implementation of two saturation tables was done by defining two saturation regions (SATNUM), both encompassing the entire grid block. Two pairs of SWFN and SGFN tables were defined, the first corresponding to CH₄ – Brine, and the second, CO₂ – Brine. A "SATNUM 1" is defined in region section normally and this will activate the first pair of saturation table to be used until instruction to change is given. In SCHEDULE section, when the depletion phase is finished, a BOX keyword is introduced encompassing all grid block, and "SATNUM 2" is then defined. This will overwrite the previous "SATNUM 1", and the second pair of SWFN and SGFN tables will be activated for the injection SCHEDULE section part.

3.1.3 Dynamic Model Implementation and Scenarios Design

The simulation model is designed to evaluate a CO₂ storage operation in a depleted gas reservoir. Two simulation phases are defined, in which first, three production wells (C1, C2, and C3) are used to deplete the reservoir and two injection wells (INJ1 and INJ2 or INJ3 and INJ4) are used to inject CO₂. Note that in each scenario, only one pair of injectors is used, depending in whether injection is in gas zone, or is in water zone, respectively.

To prepare the reservoir for storage, an initial production phase is implemented where the production wells produce the CH₄ gas to deplete the reservoir. The tree wells are completed with 0.19050 m internal diameter production casing and are capable to produce in a plateau for approximately 12 years, with gas rates of 1.5x10⁵ sm³/day for well C1, and 1.2 x10⁵ sm³/day for the remaining two producers, all set to meet the target rate, and constrained by the minimum BHP of 40 bar, 2 sm³ of maximum water production rate, and an economical limit of 3x10⁴ sm³/day. After all producers meet the constraint BHP condition, they stop production. For simulation stability purposes, the injectors are not initiated immediately, giving some waiting moths (depending on the scenario) before injection starts.

The production period serves two essential functions. First, it creates the necessary pore volume, or "storage space", by extracting the native hydrocarbons. Second, it establishes the initial pressure and fluid saturation conditions to be considered at the subsequent CO₂ injection phase. The reservoir pressure is reduced to a depleted pressure of approximately 40 bar. This pressure depletion creates a favorable pressure differential for injection, and it influences the initial injection dynamics and the pressure evolution of the system. Modeling this depletion phase, is to ensure the establishment of conditions representing a depleted gas field for a CCS project.

Subsequently, CO₂ injection is initiated via the injection wells INJ1 and INJ2 or INJ3 and INJ4 (depending on injector location), where two scenarios are implemented: first, the injectors are in the gas zone, and in another scenario, the injectors are located and completed in water saturated zone. During injection, the production wells are totally and permanently closed.

The injector well is controlled by a target injection rate, with a maximum bottom-hole pressure constraint to the initial reservoir pressure to prevent compromising the integrity of the caprock (Rutqvist, 2012). WELLSTRE keyword is used to define the components of the fluid to be injected (0% CH₄, 100% CO₂ and 0% H₂O).

In all scenarios, a fixed amount, 10⁵ tons/year of CO₂ is injected during same period of 10 years. This was strictly secured to ensure that the ultimate amount of CO₂ dissolved in water can be compared among different injection scenarios.

For all cases scenarios, after the 10 years of injecting CO₂, the injectors are stopped, and the simulation continues running for a period close to 100 years to evaluate the CO₂ dissolution behavior.

3.1.4 Simulated scenarios

To be able to compare the amount of dissolved CO₂ in brine, different simulation scenarios are considered. A base case is defined to stablish a baseline. The initial gas production phase will be kept unchanged for all cases to establish a consistent reservoir state before injection. For the sensitivity scenarios, different geological setups and injection well locations will be considered. The geological variations are represented by modeling different analytical bottom aquifer strengths, while the operational strategy is varied by changing the placement of the injector wells: varying from placing in gas zone, or in water zone.

a) Base Case (No Aquifer)

This scenario models the reservoir as a completely closed, volumetric system with a depletion drive mechanism. It is considered as a base case to quantify the natural dissolution capacity provided exclusively by the finite volume of in-situ brine. Tree producers deplete the reservoir, then, two injectors are placed in gas zone to inject 10⁵ tons/year of CO₂ for 10 years. This mass quantity is converted into volume by dividing it with density of CO₂ at standard condition (1.98 kg/m3) and subsequently convert the volume into daily injection well rate, by dividing with 365 days of the year. Note that the injectors are completed only in first entry cell to ensure no encroached (that could possibly encroach during depletion) water interferes in the scenario. Figure 17 shows clearly that injection well INJ2 is not affected by water encroachment after depletion, before CO₂ injection starts. Note that this well is the one at risk of being affected by water table rise. INJ1 is comparatively far from water gas contact.

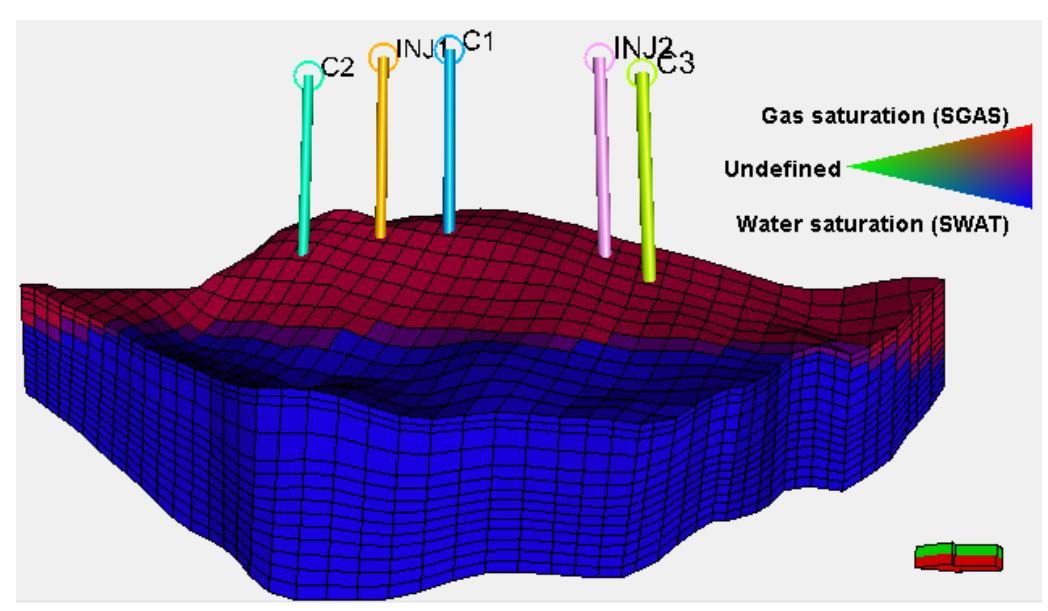


Figure 16: Wells placement in base case scenario: injectors in gas zone

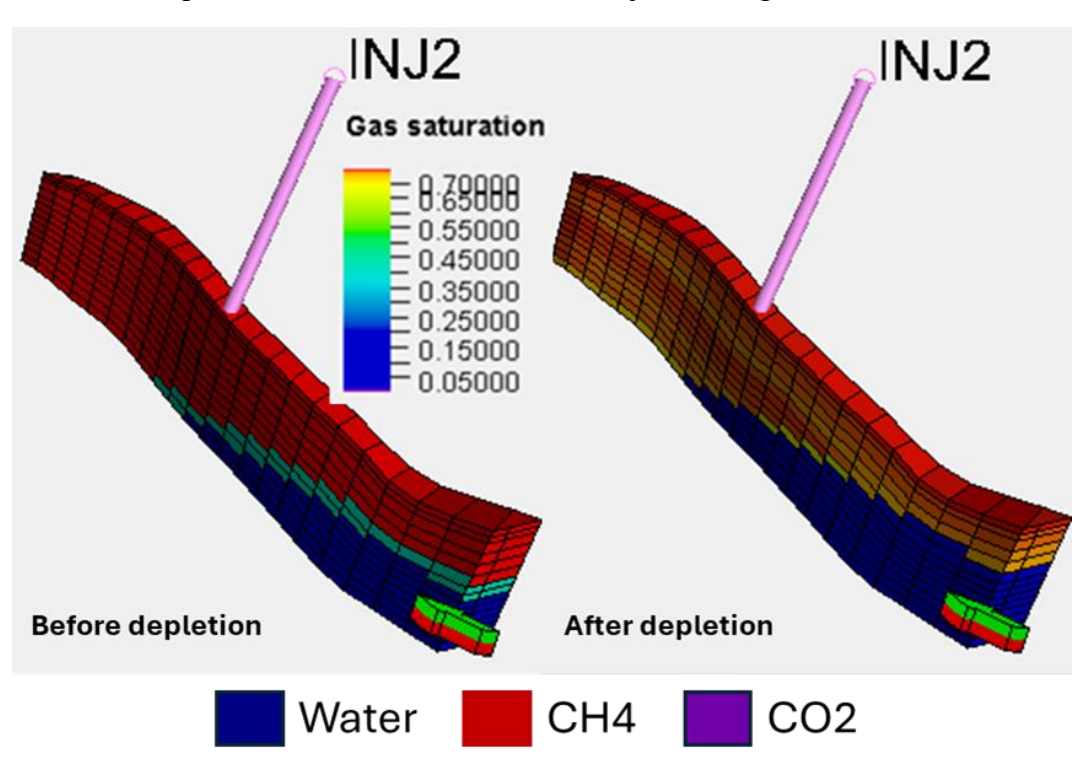


Figure 17: Injection wells not flooded by encroached water after depletion

b) Weak aquifer + injector in gas zone case

From the base case model, a moderate pressure support is modeled by introducing a weak analytical aquifer connected from the bottom of formation (from bottom layer of the reservoir), with a modest straight defined by limited porosity, small radius and thin thickness, representing a reservoir connected to a less transmissive aquifer. The injectors are in gas zone as per base case. The figure 18 confirms the effect of active analytical bottom aquifer on moving upward the WGC however, up to the end of depletion phase, no water has reached the injection wells.

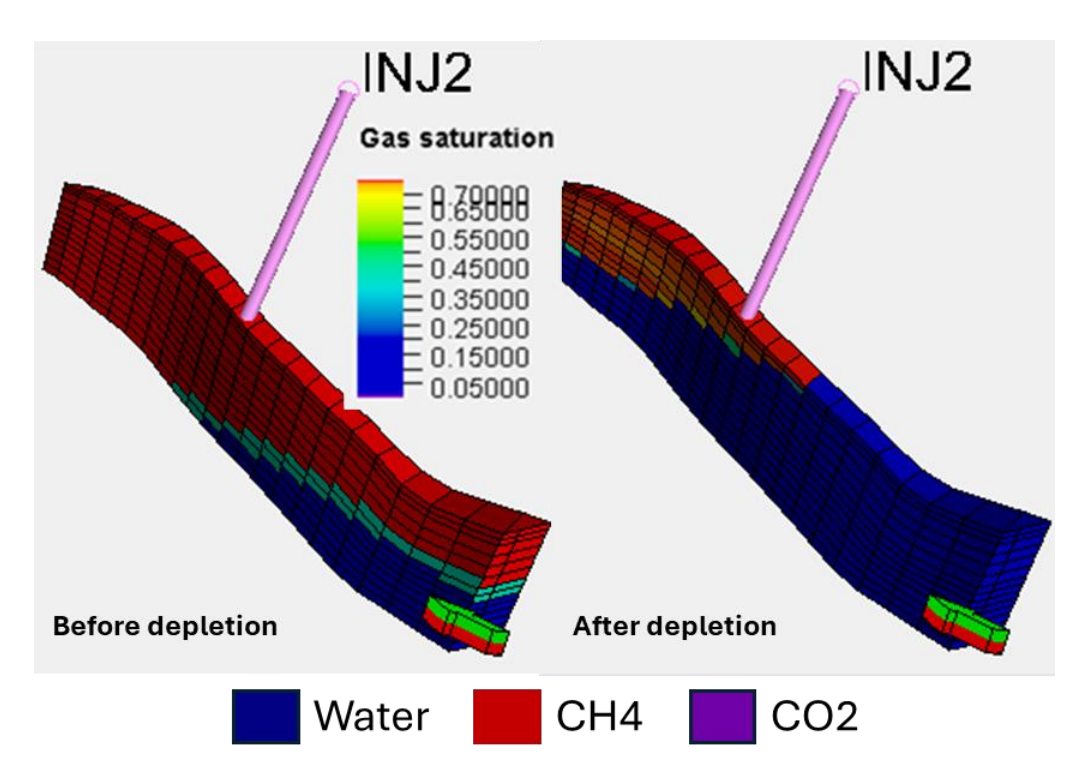


Figure 18: Injection wells not flooded by encroached water after depletion in presence of a weak bottom aquifer

c) Strong aquifer + injectors in gas zone

In this scenario significant pressure support is introduced to model a reservoir in communication with a large, and strong analytical bottom aquifer. The injectors are in gas zone exactly in same location and completion as the base case. Despite strong impact of aquifer on water encroachment, injection wells are not flooded before injection starts. See figure 19

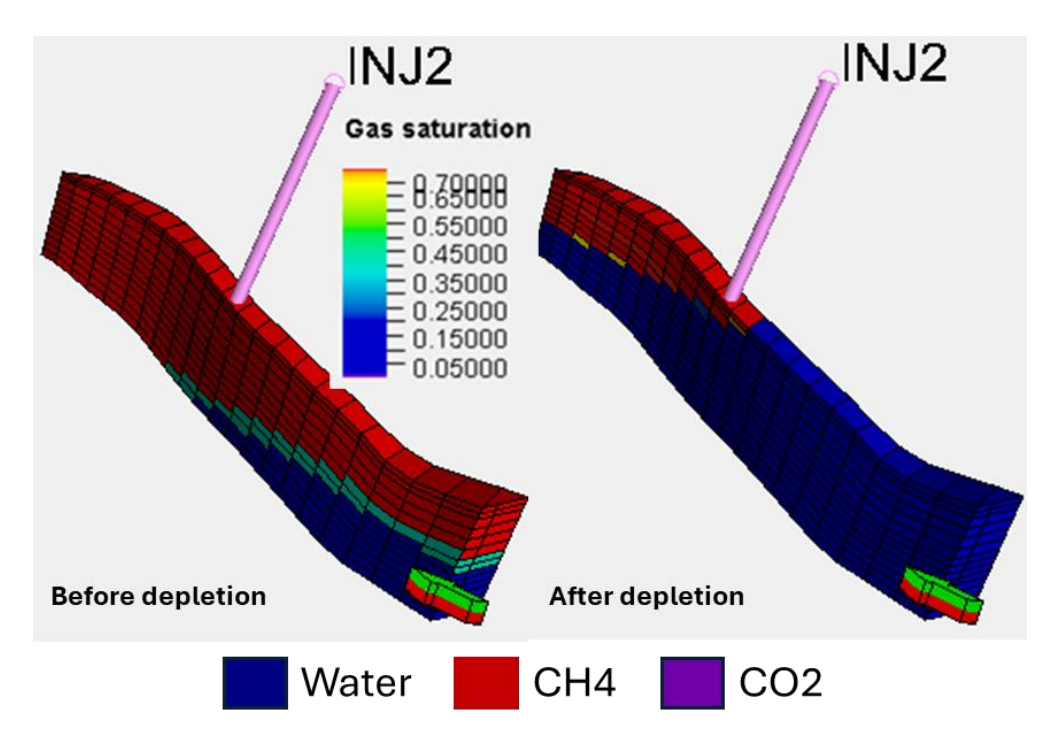


Figure 19: Injection wells not flooded by encroached water after depletion in presence of a strong bottom aquifer

d) Base case + injection in water zone (No aquifer)

The injectors are placed and completed in the water-saturated portion of the formation, below the original GWC. This scenario keeps all the base case set ups, modifying only the injection point. In this way, is expected that immediate and direct contact between the injected CO₂ and the formation brine will be possible.

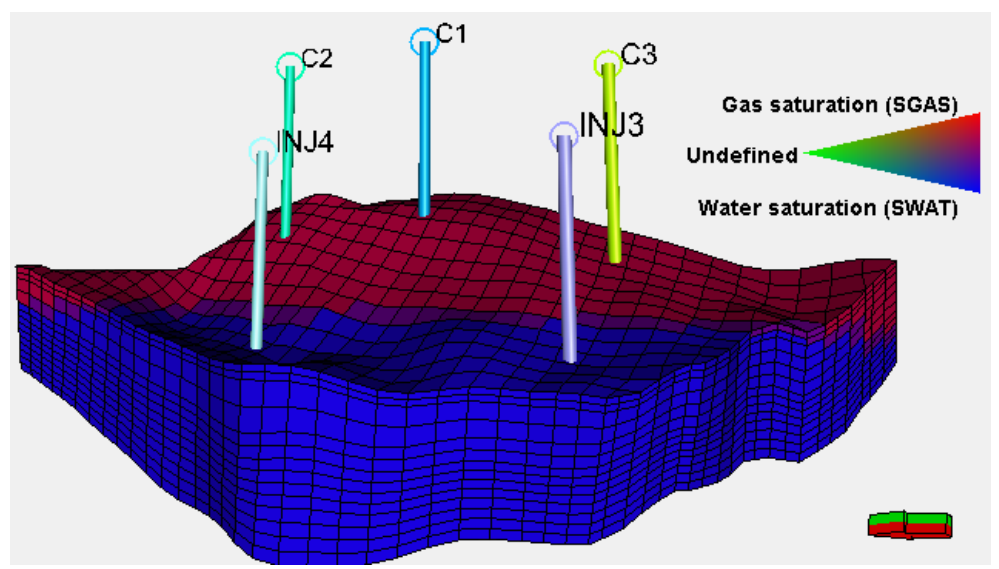


Figure 20: Wells placement in base case scenario: injectors in water zone

e) Weak aquifer + injector in water zone case

From the case described in c), the injectors are changed to be in water zone. All the other previous set ups are kept the same as per c).

| | Perm. (mD) | Poro. (%) | Cont. Angle | Thickness (m) | Radius (m) |
|-----------------|------------|--------------|----------------|------------------|---------------|
| Weak Aquifer | 100 | 10 | 120 | 50 | 80 |

Table 5: Weak aquifer parameters

f) Strong aquifer + injectors in water zone

In this scenario the strong pressure support from previous e) case is kept unchanged, and the injector wells are placed in the water zone, in the same location as all the previous water zone injection cases.

| | Perm. | Poro. | Cont. | Thickness | Radius |
|-------------------|-------|-------|-------|-----------|--------|
| | (mD) | (%) | Angle | (m) | (m) |
| Strong Aquifer | 400 | 30 | 180 | 80 | 160 |

Table 6: Strong aquifer parameters

3.2 Results discussion

a) Depletion phase

Prior to make any analyze on the main objective of this investigation, there is a need to be sure the primary depletion phase is responding as per the expectation. The figure 21 illustrates gas production profile at field scale for all the described case scenarios. In (1) are overlapped the two cases with strong aquifer; in (2) are overlapped the two cases with weak aquifer; in (3) the base case (in red) is overlapped with the scenario in which the injectors are in water zone. This confirms the depletion phase is honouring the setups proposed, where the main variation is incorporation of a bottom aquifer (a weak and strong aquifer scenarios).

In (4) are overlapped all case's injection profiles at field scale. Remember, in all cases, same amount of CO₂ is injected (10⁵ tons/year for 10 years). The conversion from mass of CO₂ to volume, is made considering CO₂ density at standard condition of 1.98 kg/m³, then, to calculate daily injection rate, the annual volume is divided by 365 days. The injectors are assigned same rate of 69185 sm³/day.

In all the cases, the injectors are capable to deliver the desired amount without reaching the maximum allowed bottom hole pressure of 200 bar.

In figure 22, the cumulative water production is added. In (5) are practically overlapped the two cases with strong aquifer, and in (6) are totally overlapped the two cases with weak aquifer. The four cases with aquifer present considerable water

production due to water gas contact rise until reaching producers, while the case with no aquifer shows practically no water breakthrough.

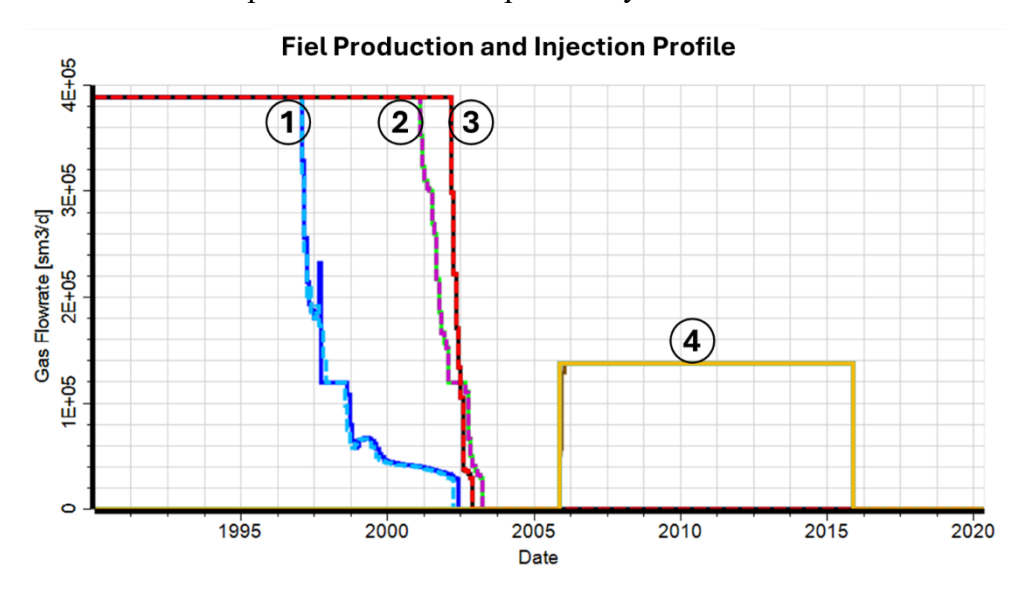


Figure 21: Field gas production and CO2 injection profiles

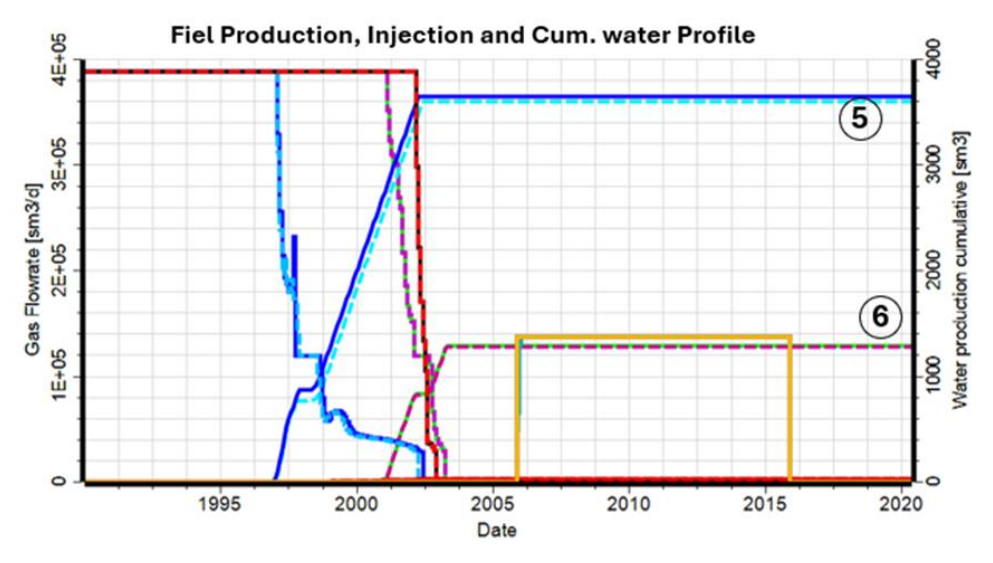


Figure 22 Field gas production and CO2 injection profiles with correspondent cumulative water production

In table 7 are summarized the plateau duration, the cumulative water production and recovery factor for the depletion scenarios. In scenarios with a bottom aquifer, plateau and recovery are less compared to cases with no aquifer as already seen in

figure 21. The cumulative water produced is higher in strong aquifer cases, moderate in weak aquifer, and practically negligible in the case of no aquifer. This is expected result in gas reservoir as active aquifers tends to encroach water in gas zone during production, making immobile all the gas that was not yet produced from the invaded zone, and once the water table reaches the well, it anticipates its closure.

| Case | GIIP (sm3) | Plateau (years) | Cumulative water prod. (sm3) | RF (%) |
|---------------------------------------|---------------|--------------------|------------------------------|-----------|
| Base Case and Base case +Inj.in water | | 12 | ~36 | ~81 |
| Weak aquifer cases | 2.2E+9 | 11 | ~1300 | ~79 |
| Strong aquifer cases | | 7 | ~3600 | ~55 |

Table 7: Plateau duration and recover factor

b) Pressure profile in different phases of simulation

In figure 23 are illustrated the field pressure profiles in all stages of the simulations. In (1) pressure decreases as response to gas production. Rapid depletion is seen in the scenarios without aquifers, and with a weak aquifer, while in strong aquifer cases, there is a clear pressure support. In (2) there is a pressure rise as response to CO₂ injection. Note that in none of the cases the initial pressure of 200 bar is reached during injection even if apparently the strong aquifer case reaches maximum pressure very close to 200 bar. The maximum pressure limit does not influence on CO₂ injection. Finally, in (3) there is a pressure stabilization when no well is active.

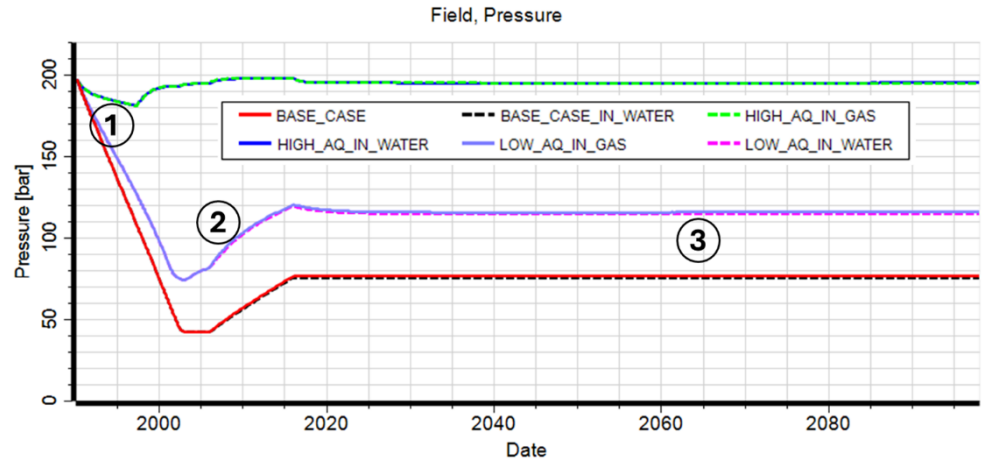


Figure 23: Pressure profile at field scale

c) Saturation distribution in different scenarios at different simulation timesteps

In figures 24 and 26 are represented the entire maps of saturation distributions of all scenarios in different timesteps, while figures 25 and 27 are the correspondent cross-sections selected at INJ2 and INJ3 injection wells respectively. Below are details of the main findings from the figures:

Line A) is the base case described in time:

- In (1) before depletion reservoir fluids in dynamic equilibrium, water in blue, CH₄ gas in red, and one transition zone in light blue.
- In (2) after depletion and before injection reduction on CH₄ gas saturation, with no rise of water gas contact.
- In (3) when injection stop CO₂ plume distributed in most of the residual gas zone and slightly invading the water zone.
- In (4) at end of simulation approximately 100 years after stopping injection, CO₂ plume continued to spread even invading more the water zone.

Line B) is the weak aquifer case with injectors in residual gas zone. The timesteps are as per A).

- In (1) before depletion reservoir fluids in dynamic equilibrium, water in blue, CH₄ gas in red, and one transition zone in light blue.
- In (2) after depletion and before injection reduction on CH₄ gas saturation, with rise of water gas contact.

- In (3) when injection stop CO₂ plume distributed in most of the residual gas zone and slightly invading the water zone.
- In (4) at end of simulation approximately 100 years after stopping injection, CO₂ plume continued to spread even invading more the water zone.

Line C) is the strong aquifer case with injectors in residual gas zone. The timesteps are as per A).

- In (1) before depletion as per A)
- In (2) after depletion and before injection as per B) with additional water gas contact rise.
- In (3) when injection stop as per B) however, lower spreading is noticeable in the residual gas zone. It may indicate that more CO2 once in contact with brine, is immediately dissolved.
- In (4) at end of simulation as per B).

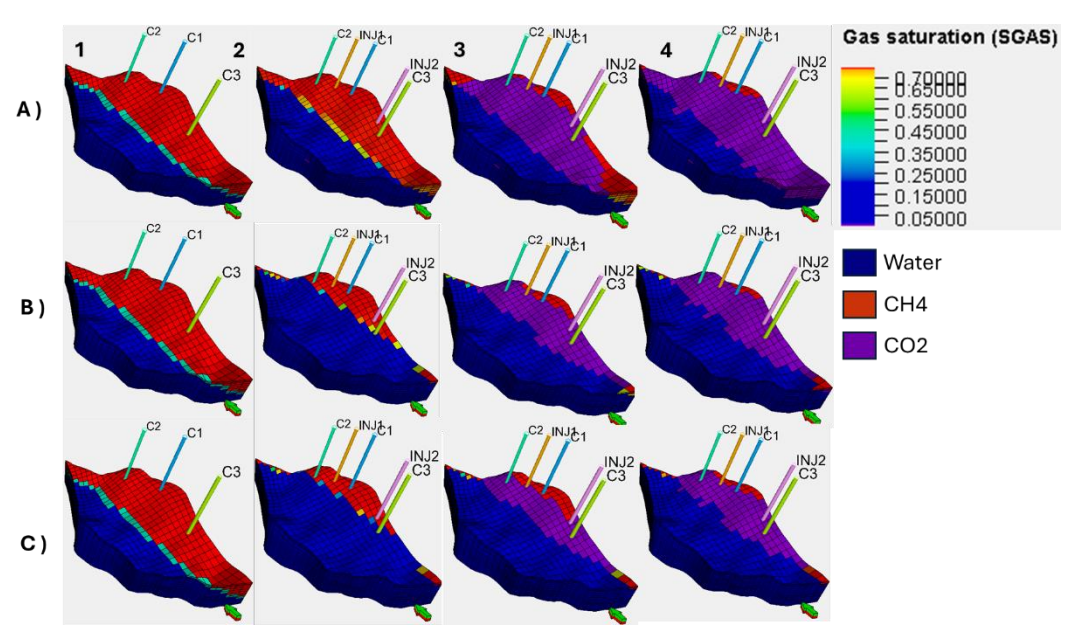


Figure 24: Saturation distribution on scenarios with CO₂ injection in gas zone

The lines A1), B1), C1) of the figure 25, are correspondent to lines A), B) and C) of the figure 24, respectively. The cross-sections are aimed to visualize the vertical distribution of the injected CO₂ on different scenarios at different timesteps

of simulation. The interpretation and findings are as per ones made for the correspondent maps, for the injection in gas zone cases.

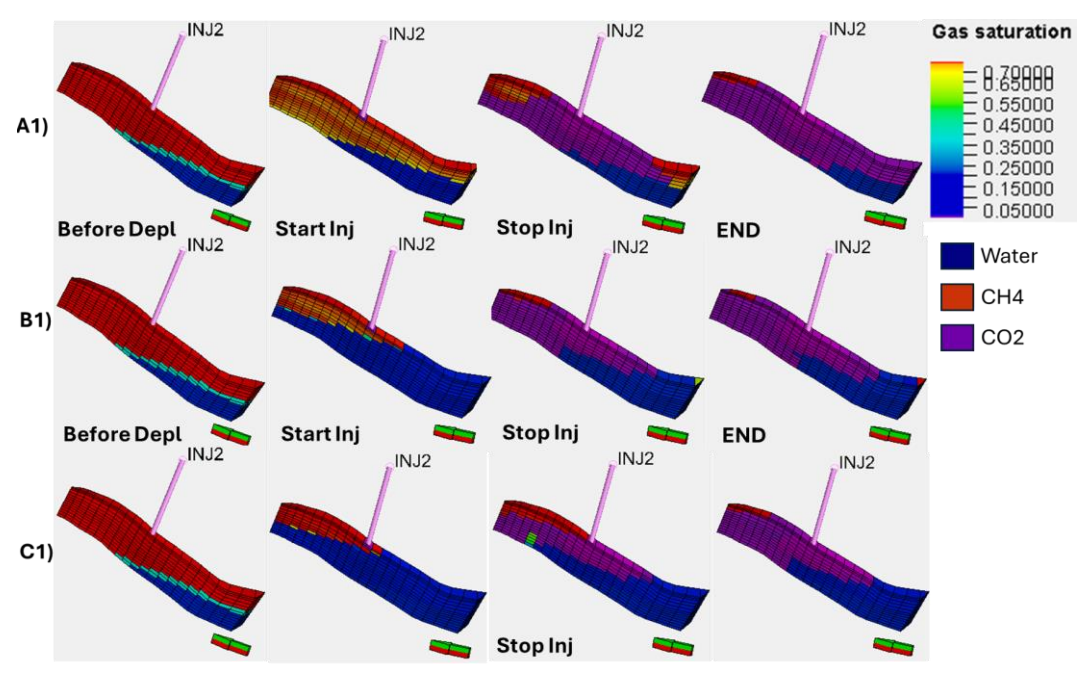


Figure 25: Saturation distribution on scenarios with CO₂ injection in gas zone, one representative cross-section selected.

Line D) is the base case plus injection in water zone, described in time:

- In (1) before depletion as per A)
- In (2) after depletion and before injection as per A)
- In (3) when injection stop CO₂ plume distributed in part of the water zone, moving toward upper part and spreading more in residual gas zone.
- In (4) at end of simulation approximately 100 years after stopping injection, CO₂ plume continued to spread covering most of the gas zone.

Line E) is case with weak aquifer, plus injection in water zone, described in time:

- In (1) before depletion as per A)
- In (2) after depletion and before injection as per B)
- In (3) when injection stop as per D) with additional plume coverage in gas zone due to water gas contact rise.
- In (4) at end of simulation approximately 100 years after stopping injection, CO₂ plume continued to spread covering most of the gas zone.

Line F) is case with strong aquifer, plus injection in water zone, described in time:

- In (1) before depletion as per A)
- In (2) after depletion and before injection as per C).
- In (3) when injection stop as per E).
- In (4) at end of simulation as per E)

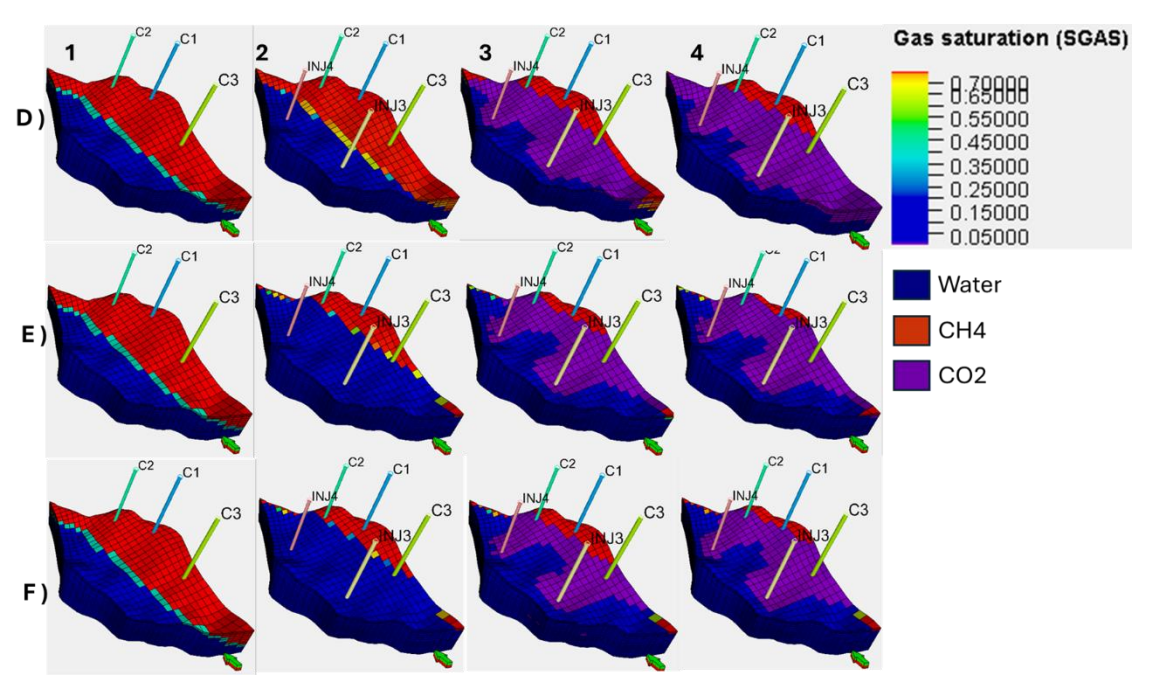


Figure 26: Saturation distribution on scenarios with CO2 injection in water zone

The lines D1), E1), F1) of the figure 27, are correspondent to lines D), E) and F) of the figure 26, respectively. The cross-sections are taken for the INJ3 injection well located in water zone and aimed to visualize the vertical distribution of the injected CO₂ on different scenarios at different timesteps of simulation. The interpretation made for the maps when injecting from water zone, are conserved. The main additional finding confirmation that when CO₂ is injected in water zone, it is buoyantly moving toward the upper part of the structure. In fact, in the maps, when CO₂ is injected from the water zone, we do not see considerable lateral dispersion in the injection point. This occurs only after the plume reaches the top of the structure (the gas zone in red).

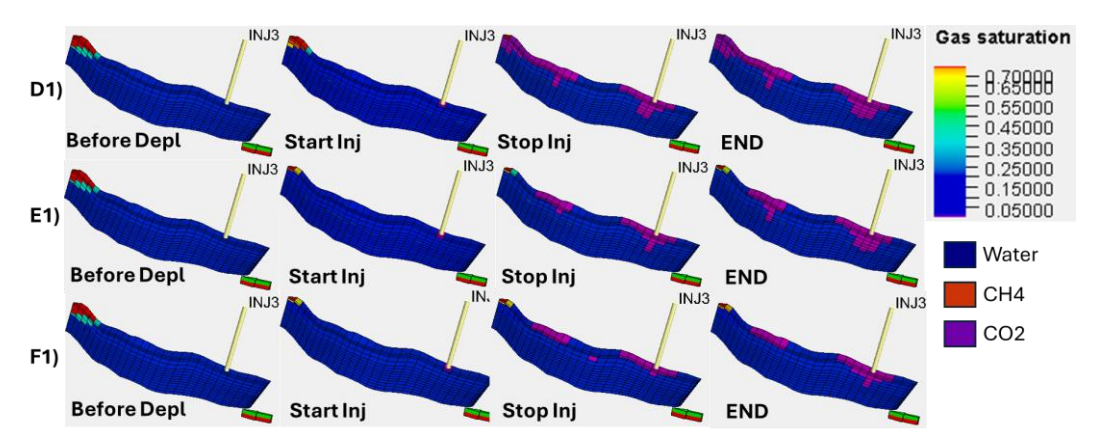


Figure 27: Saturation distribution on scenarios with CO2 injection in water zone, one representative cross-section selected.

d) CO2 component dissolved in brine

To make easy and logical comparison in the CO₂ dissolution profile, the scenarios will be grouped in two plots. First plot is the figure 28, that illustrate the tree cases where the injectors are in gas zone, varying the presence and strength of analytical bottom aquifer. In red is the base case, without aquifer. This is the case with a depletion drive mechanism and with higher recovery factor during gas production phase. It clearly shows higher amount of CO₂ dissolved when it is compared with the similar cases in which aquifer is added. This phenomenon is explained by the fact that active aquifer provides a pressure support during depletion phase leading to water encroachment (WGC rise invading the gas zone). This water rise traps the native CH₄ gas that will become additional residual CH₄. The residual native gas mix with injected gas forming a CH₄-CO₂ mixture. In this mixture, the partial pressure of CO₂ decreases with higher residual CH₄ saturation, and as partial pressure is directly proportional to CO₂ dissolution, higher aquifer strength will lead to lower dissolution. This phenomenon was extensively studied and described by Lyu et al. (2024).

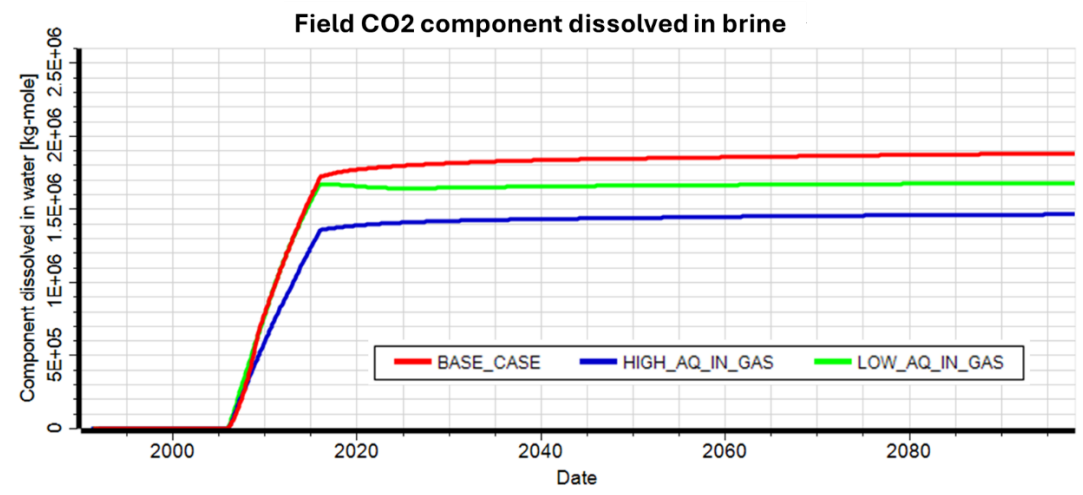


Figure 28: CO2 dissolved in brine. The cases in which the injectors are in gas zone

Second, is the figure 29 that shows the molar amount of CO₂ dissolved when the injectors are in water zone. It is seen that when CO₂ is injected directly in brine, dissolution is quicker and the ultimate amount of CO₂ that is dissolved is higher than when the injectors are in gas zone. However, when CO₂ is injected into the water zone, the influence of the aquifer strength is nearly negligible. The three water zone injection lines are closely clustered, showing only marginal differences in final dissolved molar amount.

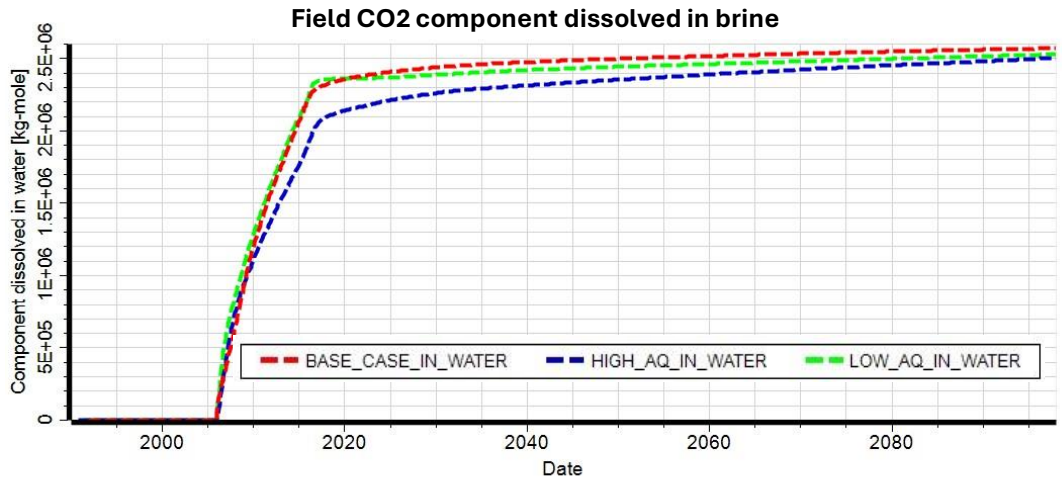


Figure 29: CO₂ dissolved in brine. The cases in which the injectors are in water zone

The plots in figure 28 and figure 29 are giving the amount of CO₂ kg-moles dissolved in brine. This does not correspond immediately to the mass or volume of dissolved gas. Instead, by multiplying these kg-mol with CO₂ molecular weight (44,009 kg/kg-mol) it results in mass of CO₂ dissolved. Then, it is easy to calculate the percentage of dissolved mass, with respect to total injected mass (10⁶ tones in total of 10 years injecting 10⁵ tones/year). Knowing the mass of CO₂ dissolved, it can easily be converted into a volume by dividing with CO₂ density at standard conditions (1.98 kg/m³). Example of how dissolved mass and volume are calculated from the molar amount of CO₂ dissolved considering base case:

$$1800574 \, Kg - mol \times 44.009 \frac{kg}{kg - mol} = 79241461 kg$$

$$mass \, of \, CO_{2 \, dissolved} \approx \mathbf{79241} \, tons$$

$$V_{CO2 \, dissolved} = \frac{m_{CO2 \, dissolved}}{\rho_{CO2}} = \frac{79241461 kg}{1.98 \frac{kg}{m^3}} = V_{CO2 \, dissolved} = \mathbf{40,020,939} \, m^3$$

Note that in the table 8 is included the amount in tones of CO₂ that remains in gas phase. These values are calculated by subtracting to the total CO₂ injected (10⁶ tones), the amount that was dissolved in brine, in each scenario. See formula (9) below:

Free
$$CO2\ Gas = Total\ Injected - Total\ Dissolved$$
 (9)

This is true if we consider that in the first decades after injection stops, the main trapping mechanisms operating are structural trapping and solubility trapping, hence, neglecting the marginal impact produced by all other trapping mechanisms. Given this assumption, the remained CO₂ in free gas phase reported in the table, is

a good approximation, not accounting for CO₂ that was residually and minerally trapped.

| Case | Cumulative CO ₂ dissolved (x10 ³ Tones) | Free gas CO ₂ (x10 ³ Tones) | Injected CO ₂ that dissolved (%) |
|------------------------------|---|---|---|
| Base case | 79.241 | 920.759 | 7.92 |
| Weak aquifer + Inj.in gas | 74.270 | 925.730 | 7.4 |
| Strong aquifer + Inj.in gas | 60.313 | 939.687 | 6.03 |
| Base case + Inj.in water | 108.437 | 891.563 | 10.84 |
| Weak aquifer + Inj.in water | 107.803 | 892.197 | 10.78 |
| Strong aquifer+ Inj.in water | 105.881 | 894.119 | 10.59 |

Table 8: Summary of CO2 mass dissolved in each simulation scenario

Conclusion

This investigation applied a rigorous numerical simulation methodology using the ECLIPSE®-300 compositional reservoir simulator to evaluate CO₂ injection strategies within in a depleted gas reservoir. PETREL® software was used to visualize the results. The study was executed by mean of designing and analyzing multiple modeling scenarios and comparing the effects of injection location (injection in residual gas zone or in water zone) and the influence of varying analytical bottom aquifer strengths on long-term storage mechanisms.

The analysis was done assuming that during simulation period, the main trapping mechanisms operating are structural and solubility trapping, hence, the impact of the other trapping mechanisms that may be acting, is assumed negligible.

A synthetic and simplified gas reservoir model was used. Depletion phase was implemented prior to CO₂ injection, and depending on model scenario, different recovery factor was observed. The simulation scenario where depletion drive mechanism was applied, higher recovery factor was observed, in line with expectation in these cases. Scenarios with strong aquifer showed lower recovery factor due to gas entrapment in invaded zone by water encroachment. After depletion, same amount of CO₂ (10⁶ tones) was injected in all studied scenarios, with same injection rates and same duration under same maximum BHP injection constraints. In none of the scenarios the initial reservoir pressure was reached during injection. After injection ceased, the simulations were allowed to continue running for a long period of approximately 100 year and the amount of CO₂ dissolved was quantified and compared among different scenarios.

The main results demonstrated that the injection of CO₂ directly into the water zone, below the GWC is the best strategy for maximizing CO₂ dissolution in

formation brine. This approach gets benefit of immediate contact between injected CO₂ with the in-situ brine resulting in efficient dissolution.

Furthermore, when the injection wells are in residual gas zone, the presence of a strong aquifer-maintained reservoir pressure causing greater water influx, causing gas entrapment and higher residual native gas saturation, that lowers the dissolution of injected gas. This phenomenon was described in literature to be related to a decrease on partial pressure of CO₂ when it gets mixed with the residual CH₄ gas (stronger aquifer, more residual CH₄ gas in reservoir hence, lower CO₂ dissolved).

After approximately 100 years post-injection, the highest amount of CO₂ dissolution reached around 11% of the total amount injected, and the lowest achieved was 6%.

The main conclusion of this thesis work is that the optimal storage plan to enhance CO₂ dissolution in the formation brine of depleted gas reservoirs involves targeting the underlying brine volume for injection. This strategy successfully leverages the solubility trapping mechanism to provide the maximum degree of security and permanence for the sequestered CO₂.

Further investigation can be proposed to quantify the amount of CO₂ that was trapped due to residual and mineral trapping mechanisms during the analyzed timeframe.

References

- [1] Bachu, S. (2008). CO2 Storage in Geological Media: Role, Means, Status and Barriers to Deployment. *Progress in Energy and Combustion Science*, *34*, 254–273. https://doi.org/10.1016/j.pecs.2007.10.001
- [2] Gozalpour, F. (2005). CO2 EOR AND STORAGE IN OIL RESERVOIRS. 60(3).
- [3] Jeong, G. S., Ki, S., Lee, D. S., & Jang, I. (2021). Effect of the Flow Rate on the Relative Permeability Curve in the CO2 and Brine System for CO2 Sequestration. *Sustainability*, 13(3), 1543. https://doi.org/10.3390/su13031543
- [4] Lyu, X., Cen, F., Wang, R., Liu, H., Wang, J., Xiao, J., & Shen, X. (2024a). Density-Driven CO2 Dissolution in Depleted Gas Reservoirs with Bottom Aquifers. *Energies*, 17(14), 3491. https://doi.org/10.3390/en17143491
- [5] Peter, A., Yang, D., Eshiet, K. I.-I. I., & Sheng, Y. (2022). A Review of the Studies on CO2–Brine–Rock Interaction in Geological Storage Process. *Geosciences*, 12(4), 168. https://doi.org/10.3390/geosciences12040168
- [6] Benson, S. M., & Cole, D. R. (2008). CO2 Sequestration in Deep Sedimentary Formations. *Elements*, 4(5), 325–331. https://doi.org/10.2113/gselements.4.5.325
- [7] Guenther, A. B., Zimmerman, P. R., Harley, P. C., Monson, R. K., & Fall, R. (1993). Isoprene and monoterpene emission rate variability: Model evaluations and sensitivity analyses. *Journal of Geophysical Research: Atmospheres*, *98*(D7), 12609–12617. https://doi.org/10.1029/93JD00527
- [8] Jeong, G. S., Ki, S., Lee, D. S., & Jang, I. (2021). Effect of the Flow Rate on the Relative Permeability Curve in the CO2 and Brine System for CO2 Sequestration. *Sustainability*, *13*(3), 1543. https://doi.org/10.3390/su13031543
- [9] Snippe, J., & Tucker, O. (2014a). CO2 Fate Comparison for Depleted Gas Field and Dipping Saline Aquifer. *Energy Procedia*, 63, 5586–5601. https://doi.org/10.1016/j.egypro.2014.11.592

- [10] **Gassnova.** (n.d.). *Carbon capture and storage*. Norsk Petroleum. https://www.norskpetroleum.no/en/environment-and-technology/carbon-capture-and-storage/
- [11] Akai, T., Saito, N., Hiyama, M., & Okabe, H. (2021). Numerical Modelling on CO2 Storage Capacity in Depleted Gas Reservoirs. Energies, 14(13), 3978. https://doi.org/10.3390/en14133978